

## Article

# Cenozoic Marine Basin Evolution in the Western North Aegean Trough Margin: Seismic Stratigraphic Evidence

Alexandros Varesis and George Anastasakis \*

Department of Historic Geology Paleontology, Faculty of Geology & Geoenvironment, National and Kapodistrian University of Athens, Panepistimiopolis, 15784 Athens, Greece; avaresis@geol.uoa.gr

\* Correspondence: anastasakis@geol.uoa.gr; Tel.: +30-21-0727-4168

**Abstract:** This study investigates the interplay of evolving tectonic and submarine sedimentation processes in the northwest Aegean Sea using marine multichannel seismic profiles. We identify an extensive basin developing in the Thermaikos Gulf inner shelf, outer shelf, and slope leading to the 1500 m deep West North Aegean Trough (NAT). We establish the unconformable extent of Eocene and Oligocene sequences on the upper shelf and trace their continuation in the deeper shelf and slope of Thermaikos Gulf. The start of the Miocene and Middle Miocene developed below the well-established Messinian bounding reflectors that are mostly erosional. Important lateral variations are observed within the Messinian sequence, which is up to 0.8 s thick. Messinian prograding clinoforms are identified on the Thermaikos Gulf shelf and southeast of Chalkidiki, and a zone of irregular reflectors is attributed to the Messinian salt layer. The transpressional deformation of the Messinian in the southwestern margin constrains the timing of westward progradation of the North Anatolian Fault during Messinian. The Pliocene-Quaternary sediments are 0.6–1.8 s thick, showing the overwhelming effect of tectonics on sedimentation plus the northwards Quaternary activation at the Thermaikos apron.



**Citation:** Varesis, A.; Anastasakis, G. Cenozoic Marine Basin Evolution in the Western North Aegean Trough Margin: Seismic Stratigraphic Evidence. *Water* **2021**, *13*, 2267. <https://doi.org/10.3390/w13162267>

Academic Editors: Thomas M. Missimer and Kristine Walraevens

Received: 30 June 2021

Accepted: 16 August 2021

Published: 19 August 2021

**Publisher's Note:** MDPI stays neutral with regard to jurisdictional claims in published maps and institutional affiliations.



**Copyright:** © 2021 by the authors. Licensee MDPI, Basel, Switzerland. This article is an open access article distributed under the terms and conditions of the Creative Commons Attribution (CC BY) license (<https://creativecommons.org/licenses/by/4.0/>).

**Keywords:** seismic stratigraphy; Messinian evaporites; North Aegean Trough; Cenozoic stratigraphy

## 1. Introduction

In the Aegean Sea, Cenozoic crustal extension is generally viewed as a result of escape tectonics, with the Aegean microplate pushed westward by Anatolia due to the impact of the Arabian indenter and Eurasia [1]. The Miocene collision of Anatolia with Eurasia led to crustal thickening and subsequent westward gravitational collapse and escape of Anatolia, leading to the formation of the North Anatolian Fault (NAF), which has progressively propagated, reaching the North Aegean at around 5 Ma [2–4]. It is generally accepted that decreased rates of convergence between Eurasia and Africa in the Oligocene [5] resulted in roll-back and extension in the Aegean [6]. Eocene basins are widespread in Thrace (NW Greece). The closure of the Vardar and Pindos Oceans produced an area of thickened continental crust and led to thrust migration westward through the external Hellenides. This Mesohellenic orogenesis [7] established the drastic sedimentation centers of the Mesohellenic basin. Dinter [8] has argued that similar Middle–Late Eocene continental subduction took place in the Rhodope. Traces of Eocene ophiolite obduction may be seen to the west and south of the North Aegean Trough (NAT), e.g., in the Pelion and North Sporades Islands [7], while molasse was already deposited in the hinterland basins.

Voluminous igneous activity has shifted southward through the Cenozoic, from North mainland Greece (Eocene–Oligocene plutonism and volcanism) through the widespread volcanism of the North Aegean islands and the plutonism in the Central Aegean Sea to the present-day active Pliocene-Quaternary South Aegean Volcanic Arc. Throughout the Miocene, a discrete West Aegean crustal block rotated ca. 30° clockwise, marking the junction of the East Aegean–Anatolian block with the Central Aegean [9]. A drastic change

occurred in the early Miocene, as manifested by rapid SW-directed extension, recognized both in North Greece and the central Aegean islands. Essentially, this stretching was controlled by roll-back of the Hellenic subduction zone and was less pronounced in Minor Asia due to the presence of the Mendere block [10]. The early Miocene Symvolon rupture, in the Kavala coastal region, probably was a divergent system, including the Thasos Island detachment extending to low-angle faults in the Olympos mountain region. Dinter [8] correlated the volcanism with the early Miocene extension on the Symvolon shear zone and Thasos detachment. Local early Miocene sedimentation is known from the Kavala–Thasos region and Katerini to the east of Olympos–Ossa–Pelion mountain range.

Despite the high interest in the complex geological history of the North Aegean, the constraints of the offshore stratigraphic framework of the area remain a key issue, especially in its western extremity. Apart from the extensive commercial petroleum exploration activity in the 1960s and 1970s, the majority of the seismic surveys covering the western regions of the NAT were limited in the investigation of the shallower formations mainly due to the utilization of single-channel seismic systems.

The stratigraphic framework of the offshore regions and the timing of extension events in the North Aegean can be more accurately determined by correlating land facies stratigraphy to the offshore basin seismic stratigraphy as controlled by available drillhole data. In this study, we interpret a suite of reprocessed legacy multichannel seismic reflection profiles, covering roughly the area within and around the western half of present-day North Aegean Trough. The area of interest is bounded to the north by the broad Thermaikos Gulf continental shelf and the peninsula of Chalkidiki, to the west by the Hellenic hinterland, and to the south by the continental shelf of the Sporades Islands (Figure 1). The length of the western part of the trough is approximately 170 km, and it displays a maximum width of 70 km. The seafloor morphology is rather complex with several local bathymetric deeps of more than 1500 m [11]. Although we do not possess direct drillhole control of the seismic reflectors, we cross-correlate observed reflector depths to adjacent wells retrieved in the outer Thermaikos Gulf shelf and coast.

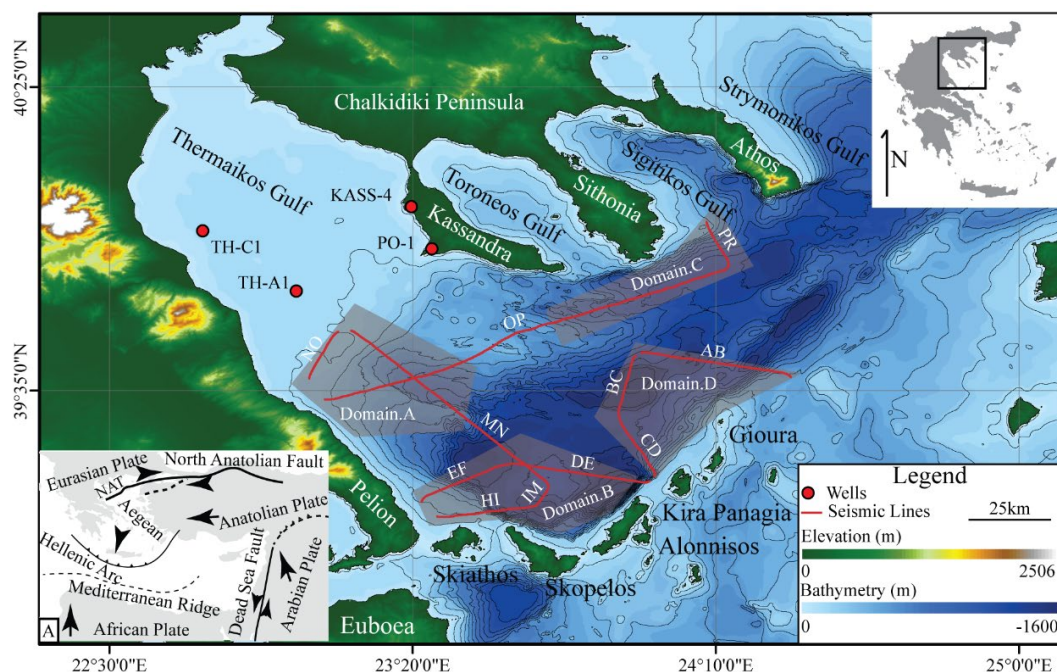


**Figure 1.** Bathymetry of the area around the western half of North Aegean Trough. The seismic lines acquired during SeisGreece mission analyzed in this study are shown. The shaded areas correspond and constrain the domain distinguished. (A) Schematic illustration of the major geodynamic interactions of the tectonic plates in the area of Eastern Mediterranean (modified after Taymaz et al. [12]). The wells in the outer Thermaikos shelf and Kassandra Peninsula are indicated. Well names: Thermaikos-C1 (TH-C1), Thermaikos-A1 (TH-A1), Posidi-1 (PO-1), and Kassandra-4 (KASS-4).

## 2. Regional Setting

### 2.1. Regional Tectonic Setting

The geodynamic evolution of the broad area of North Aegean has been associated with the relative kinematic interactions among the Eurasian, African, Arabian, and Anatolian plates (Figure 1A). The subduction of the African plate under the Eurasian creates the Hellenic Arc retreat and, as a result, an extensional regime in the North Aegean [13]. In parallel, the northern movement of the Arabian plate through the Dead Sea Fault (DSF) affects the Anatolian plate, which through the North Anatolian Fault (NAF) propagates westward, affecting the Aegean [3,12,14].

The back-arc extension of the Aegean was likely initiated during the Middle Eocene [15]. The localized deformation is associated with the creation of Paleogene sedimentary basins in the northern and central parts of Aegean containing Middle Eocene and/or Oligocene sediments [16].

The Neogene tectonic development is established based on several marine geophysical studies [17–21], aided by seismological and fault plane solution research [22–24], offshore fault development and distribution [25–27], and satellite geodesy [28–30]. The westward propagation of the NAF [2,4,31] has been linked with the basin development of the North Aegean Trough, where a dual structural regime has been identified (extensional tectonics with an important strike-slip component, Figure 2) [23,32–34]. The creation of several depositional centers reflects the intense tectonic activity in the area associated with complex fault kinematics, anticlinal and synclinal structures resulting from transpressional and transtensional dynamics (Figure 2).

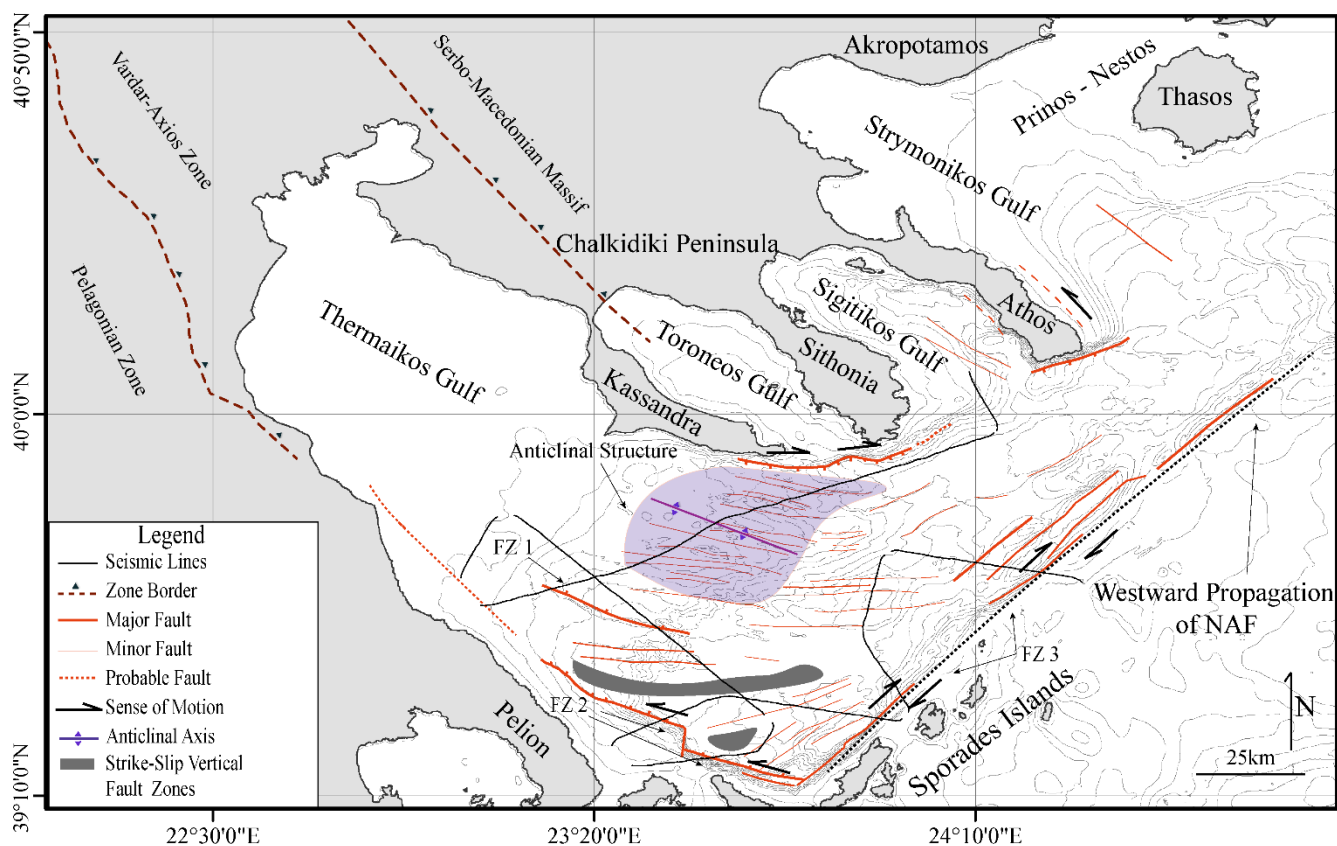


**Figure 2.** Simplified map of active tectonic lineaments in the North Aegean Trough, modified after Ferentinos et al. [35], Papanikolaou et al. [25], and Sakellariou et al. [18]. The kinematics direction is based on the cited references, while the three fault zones (FZ) deduced from the analysis of the seismic data are indicated. The purple-shaded area covers the major anticlinal structure observed in the seismic profiles. Gray-shaded areas constrain the strike-slip vertical fault zones identified by Papanikolaou et al. [25] and are further correlated in the present study. The location of the seismic lines is also shown.

## 2.2. Regional Cenozoic Stratigraphy

Our knowledge regarding the Paleogene deposits in North Aegean and the western NAT is derived by the investigation of offshore and onshore exploration wells along with the paleogeographic extent of the Axios basin and their correlation with seismic surveys, mainly in the broad area of the Thermaikos Gulf and the Chalkidiki Peninsula. Onshore well KASS-4 (Figure 3) drilled on the NW coast of the Kassandra Peninsula of Chalkidiki retrieved a thick sequence of 1350 m of Oligocene age deposits essentially consisting of fine-grained claystones and siltstones indicative of a hemipelagic depositional environment. Underlying this unit, a series of Eocene age formations is reported (320 m) with alternations of sandstones and siltstones transitioning from coarse- to fine-grained marine depositional cycles. The southern well PO-1 at Possidi, on the Kassandra Peninsula, penetrated a thick package of 2230 m of Oligocene clastic formations consisting of sandstones, claystones, and siltstones, overlying a series of 380 m of Eocene age sediments dominated by the presence of fine-grained sandstones and siltstones [36,37]. The Middle-Upper Eocene formations in these wells reflect the transition from lacustrine and shallower marine environments (sands, lignite, and shales) to hemipelagic settings toward the south (alternations of sandstones to clay turbidites and shales). This shift in the depositional setting has been linked with increased sea levels due to transgressions and increasing basin subsidence [36]. A coeval alteration in the paleoenvironmental setting was reported in the study of Paleogene deposits by IFP [38], where the level of Upper Eocene–Oligocene marks the transition of hemipelagic to brackish depositional settings (Figure 3A).

The results of offshore wells in the outer Thermaikos Gulf were debated among the interpretations of Faugères and Robert [39] and Lalechos and Savoyat [40]. Following the interpretation of the latter, in the offshore well TH-C1 (Figure 3), a Middle Eocene series of an approximate thickness of 550 m has been identified, characterized by a clastic series of micro-granular sandstones, clays, and siltstones. Below this unit, a series of 260 m of basal conglomerate with quartz, marble, and serpentinite clasts with interlayered sandstones and clays is attributed to the Eocene age. The correlative top of the Paleogene, several kilometers south, in TH-A1 (Figure 3), is an Upper Eocene–Oligocene 460-m-thick sequence, characterized by the presence of claystones, marlstones, and fine-grained sandstones [40].

The sediment accumulation during Neogene in the NAT is characterized by significantly thick formations (approximately 4.5 km) of the Miocene-to-Quaternary age [17,40]. More recent studies [35,41] are indicative of even greater thickness, reaching locally up to 6.0 km. The variation of the local depocenters is a direct result of the regional structural regime, creating several mini-basins [25,27].

According to the lithological descriptions of the deep wells in the broad area of Thermaikos Gulf, the Pliocene-Quaternary formations are associated with clastic deposition with alternations of marls, clays, silts, and coarser formations of fluvial sands (1065 m in TH-C1 and 910 m in TH-A1) (Figure 3). The underlying Miocene units (1537 m in TH-C1 and 2297 m in TH-A1) are linked with fluvial and shallow marine facies of marlstones with interbedded sandstones and siltstones, while thin lignite deposits are present in the Middle Miocene of TH-A1. A distinct differentiation between the two wells is evident in the termination of the Miocene deposits in TH-A1 due to the presence of a base conglomerate characterized by quartz, marble, serpentinite, ophiolite, and metamorphic rocks bounded by a compact clay–silt matrix [40].

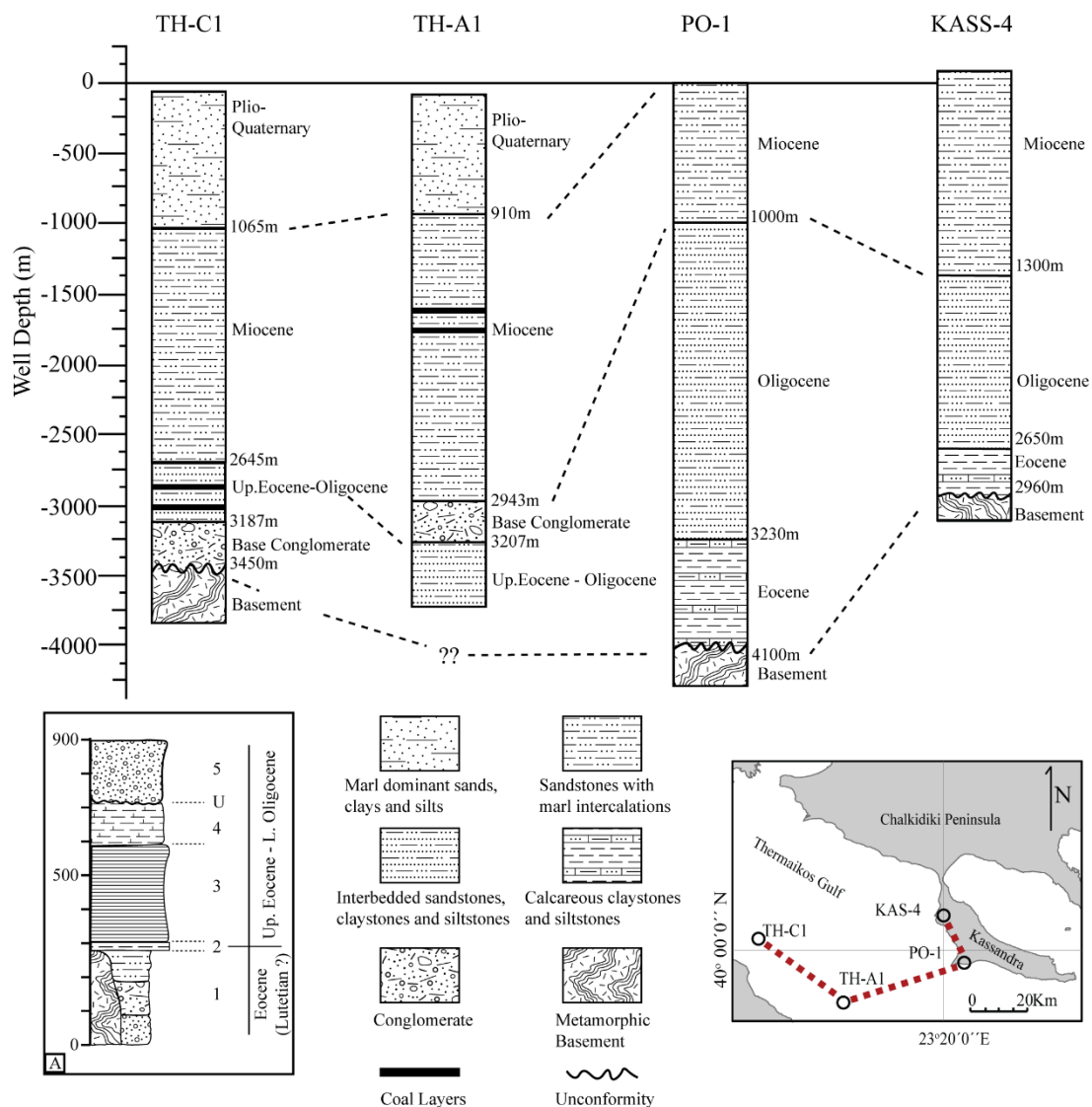


**Figure 3.** Schematic well correlation of four wells in the area of the Thermaikos Gulf and Kassandra Peninsula. The wells are modified after the integration of Faugères and Robert [39], Lalechos and Savoyat [40], and Aidona et al. [37]. (A) Synthetic stratigraphic column for the Paleogene formations in Axios basin after IFP [38]. (1) sequence of conglomerates, sands, and marls over the metamorphic basement, (2) neritic limestones, (3) marls with nummulites, (4) clay marls with ostracods, (U) unconformity, and (5) conglomerates and sandstones.

To the north of the eastern limit of the studied area, in the Nestos–Prinos submarine basins (Figure 2), there are several wells accessing the hydrocarbon plays [42,43]. Over 2500 m of post-Middle Miocene sediments have been recovered in several wells. Over the metamorphosed basement, a thick sequence of coarse-grained alluvial fan deposits including coal seams is succeeded unconformably by fine-grained marine fan deposits consisting of sand to silt turbidites and fine-grained shales. They are overlain by a zone of limestone, dolomite, and anhydrite layers alternating with clastics. Toward the deeper basinal depocenters anhydrite is replaced by salt (halite) layers, usually a few meters thick. On top of this series, an extensive dark-gray marl, strongly petroliferous with frequent turbidite intercalations, is reported [42]. Prinos basin turbidite successions are over 300 m thick. The overlying Messinian evaporitic series mostly consists of anhydrite, marls, and limestone layers 3–5 m thick, frequently alternating with evaporitic and more clastic turbidites. Within the basins, seven to eight salt layers are alternating with clastics and a total thickness of up to 800 m has been observed. Post-Messinian, Pliocene, and

Quaternary marine sediments exceed 1200–1600 m in thickness. Onshore marine Upper Miocene sediments have been described. In onshore Strymonikos Gulf, especially in the Akropotamos area (Figure 2), thin evaporites topped by an erosional surface were assigned to the first stage of the Messinian (5.97–5.5 Ma according to Snel et al. [44] and 5.97–5.6 Ma according to Karakitsios et al. [45]). Arguments are in favor of a marine gateway between the Aegean and Dacitic Paratethys basin through the Balkan Strymonikos river valley before and after the Messinian salinity crisis (MSC) [46].

### 3. Methodology

#### 3.1. Dataset and Data Processing

The studied dataset consists of 11 multichannel legacy profiles, acquired as part of the project SeisGreece that took place in 1997 in the broad area of North Aegean (multichannel streamer, 96 channels, source of 300 in<sup>3</sup>). The available seismic profiles were processed (pre-stack depth migration, PSDM, European polarity) and resampled to 8 ms by Vinger [47]. The estimated vertical resolution of the survey, based on the average dominant frequency in the studied intervals (about 25 Hz, average velocity of 2200 ms<sup>-1</sup>), yields at best a resolution of 25–30 m (one-quarter wavelength in the sense of Herron [48]). In addition to the original seismic processing, a band-pass frequency filter was applied, in parallel to a structurally oriented filter through DUG Insight™ [49]. The latter reduced the noise of the reflectors along their structural planes, as defined by a pre-calculated dip field. These two processes were evaluated as effective for the majority of the profiles as the deeper reflectors (below the first 3.5 s) were efficiently improved and the shallower ones were considerably enhanced.

#### 3.2. Domains Configuration

The acquisition track lines of the seismic profiles cover a large area, with widely spaced (~25 km) line spacing. This, in addition to the general physiographic complexity of the sea bottom, were the main reasons upon which the interpretation strategy was constrained into four areas or domains along the western half of the NAT (Figure 1). Domain A covers the inner and outer Thermaikos shelf, adjacent to the studied offshore (TH-A1 and TH-C1) and onshore wells (PO-1 and KASS-4) (Figure 3). Domain B is located in the western Sporades (Skiathos, Skopelos, Alonnisos) near the western termination of the North Anatolian Fault [18,25] where the maximum sea depth of the NAT (~1600 m) is located [11]. Domain C extends south of the Chalkidiki Peninsula continental shelf apron, while Domain D covers from the continental shelf of eastern Sporades (Kira Panagia, Gioura) to the deeper, central parts of the basin.

#### 3.3. Seismic Interpretation

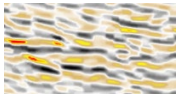
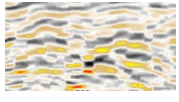
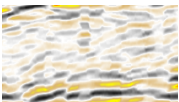
The process of seismic interpretation included (a) the recognition and mapping of the marker horizons across the distinguished domains (amplitude strength, frequency, and polarity), (b) the establishment of a stratigraphic framework through bounding horizons and reflection terminations, (c) description of the characteristic seismic facies, and (d) the identification of the respective faults, structural elements, and their apparent dip.

## 4. Results

#### 4.1. Seismic Facies

The acoustic image of the identified seismic packages alternates laterally across the studied areas. Therefore, six seismic facies (Table 1) were identified in order for the packages' optimal description. Their distinction was based on their acoustic signature, internal configuration, lateral continuity, reflector architecture, and geometry (in the sense of Sangree and Widmier [50] and Mitchum et al. [51]).

**Table 1.** Seismic facies recognized across the four domains and their definitive characteristics.

Seismic Facies	Acoustic Signature	Internal Configuration	Lateral Continuity	Reflection Characteristics	Geometry
Si		Parallel Well Stratified	High	Moderate to High Amplitude High Frequency	Sheet-Shaped Basinwards Wedge-Shaped Landwards
Sii		Subparallel to Parallel Stratified with Internal Unconformities	Medium to High	Low to Moderate Amplitude High Frequency	Sheet-Shaped Basinwards Wedge-Shaped Landwards
Siii		Subparallel to Wavy	Medium	Moderate to High Amplitude Low Frequency	Sheet to Wedge
W		Wavy to Hummocky	Poor	Low to Moderate Amplitude Low Frequency	Complex-Irregular
M		Transparent to Hummocky	Discontinuous	High Amplitude Top and Bottom Reflectors and Low Internal Low Frequency	Lens Updoming Features
Ch		Chaotic to Non-Internal Configuration	Discontinuous	Low Amplitude	No Coherent Geometry

- Seismic facies Si shows the parallel internal configuration with well-stratified reflectors of moderate-to-high amplitude and high frequency. The associated packages display high continuity of sheet-shaped geometry in the central regions of the mini-basins and a wedge-shaped closer to the slopes.
- Seismic facies Sii comprises semi-continuous to continuous subparallel reflectors, with locally observed internal unconformities. The amplitude of the reflectors is observed to be low to moderate with high frequency. They follow a sheet (basinwards) to wedge (landwards) geometry.
- Seismic facies Siii shows subparallel-to-wavy internal configuration of medium continuity with distinct variations of moderate- to high-amplitude reflectors and low frequency. It is more recognizable in the deeper locations of the mini-basin following a sheet-to-wedge shape in accordance with the terminations of the associated reflectors.
- Seismic facies W shows a seismic image of wavy-to-hummocky reflectors with complex geometry. It illustrates poor continuity with an acoustic character of low-to-moderate amplitude and low frequency.
- Seismic facies M is only observed locally, in the northeastern part of the study area, (Domain C), where the associated seismic package is constrained by high-amplitude top and bottom reflectors. The internal reflector configuration displays a transparent and hummocky image with lens geometry and updoming features.
- Seismic facies C is of low amplitude, chaotic internal configuration with discontinuous reflectors, and no clear coherent geometry. The presence of the facies is associated with areas of either a disturbed acoustic image due to tectonism or areas of no coherent geometry.

#### 4.2. Seismic Stratigraphic Framework

The local seismic stratigraphic framework was based on the identification of major seismic horizons with respect to their acoustic character, their extent along the studied areas, and the lithostratigraphic knowledge derived by the neighboring wells. The quality of the seismic dataset enabled the distinction of eight key horizons in the outer shelf of Thermaikos (Figure 4), while only four horizons (H1–H4) were mapped in the rest of the studied areas. In addition to the reflector of the sea bottom (S.B.), the combination of the mapped horizons distinguishes the studied packages into eight seismic units.

- Seismic Unit 1 (SU.1) is marked by the reflector of sea bottom and H1. It is attributed to an Upper Quaternary age and illustrates a constant seismic signature dominated by parallel, dense and high-amplitude reflectors of high frequency. The time thickness of the unit varies from 0.3 s in the northwestern margin (Domain A) to 0.9 s in the southeastern and central areas of the trough (Domains B and D).
- Seismic Unit 2 (SU.2) is marked by H1–H2 horizons and correlates with the Lower Quaternary age. The acoustic signature of the unit is dominated by a moderate variation of parallel to subparallel reflectors of high-to-moderate amplitude. The time thickness of the unit ranges from 0.45 s to more than 0.8 s in the southern areas (Domain B).
- Seismic Unit 3 (SU.3) is marked by H2–H3 horizons and attributed a Pliocene age. It illustrates parallel to sub-parallel reflectors of moderate-to-high amplitude and high frequency. The time thickness of the unit ranges from approximately 0.4 s (Domain A) to its maximum mapped thickness, near western Sporades (Domain B) reaching more than 1.5.
- Seismic Unit 4 (SU.4) is marked by H3–H4 horizons and correlates with the Upper Miocene age. The top of the unit is bounded by a well-defined, high-amplitude reflector (H3, with high regional importance as it is associated with the top surface of the Messinian), the strong acoustic presence of which is tracked, almost in all the available seismic profiles. The time thickness of the unit varies from 0.2 s to more than 0.7 s.
- Seismic Unit 5 (SU.5) is marked by H4–H5 reflectors and attributed to the Middle Miocene age. The seismic signature of the unit is characterized by semi-parallel-to-wavy reflectors of low frequency, the time thickness of which varies from 0.25 to 0.9 s.
- Seismic Units 6 (SU.6), marked by H5–H6 horizons, is attributed to the Lower Miocene age. It is characterized by low-frequency and moderate-amplitude reflectors of semi-parallel geometry, displaying a thickness of 0.2–0.5 s.
- Seismic Unit 7 (SU.7) is marked by H6–H7 horizons and correlates with the Oligocene age. It consists of semi-parallel-to-parallel, low- to moderate-amplitude reflectors of moderate frequency and continuity. Its thickness ranges from 0.25 to 0.7 s.
- Seismic Unit 8 (SU.8) is marked by H7–H8 horizons, and it is tentatively attributed to an undifferentiated Eocene age. Its reflector configuration is characterized by semi-parallel, low- to moderate-amplitude reflectors of moderate frequency and continuity. Even though it is poorly constrained, it illustrates a time thickness ranging from 0.4 s to more than 1.2 s.

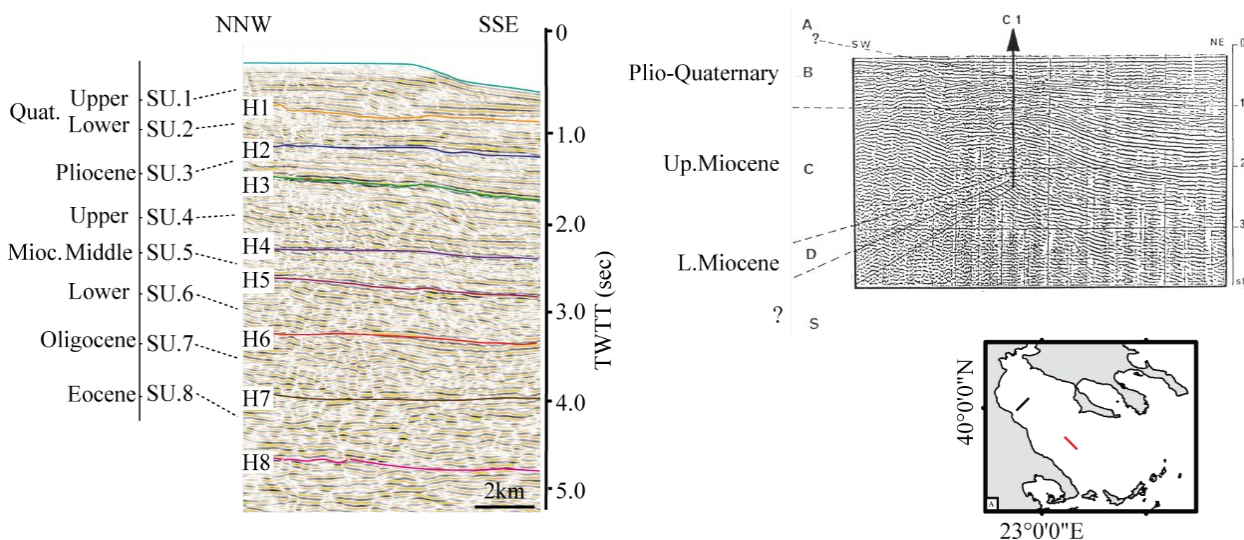


**Figure 4.** Left: seismic units’ distinction with picked horizons in part of the MN section (red line in map). Right: vintage seismic profile from north Thermaikos (black line in map) from IFP [38] correlated with well TH-C1.

### 4.3. Seismic Architecture of the Western-Central NAT

#### 4.3.1. Domain A, Thermaikos Shelf

Covered by three seismic lines (Figures 5–7), the area is associated with the transition from the inner-outer shelf of Thermaikos to the basin slope of the central parts of the western NAT. At the center of the inner shelf of the continental platform, SU.1–3 are dominated by Si and Sii facies, with a total thickness of 0.6–0.8 s. The top of SU.3 (H2) is characteristically onlapping unconformably over H3 (Figure 5). SU.4–5 are characterized by Siii facies and evident post-depositional tectonism. The bottom of SU.5 (H5) toplaps unconformably, the clearly tilted positioned, deeper formations, which illustrate Siii facies. Toward the southwestern end of the section, the unit is characterized by W facies, deformed by a characteristic concave downward geometry of H5. The latter is linked to a clear, vertical displacement of the surface, as observed by a set of normal faults mapped deforming the surface of horizon H5 (Figure 5).

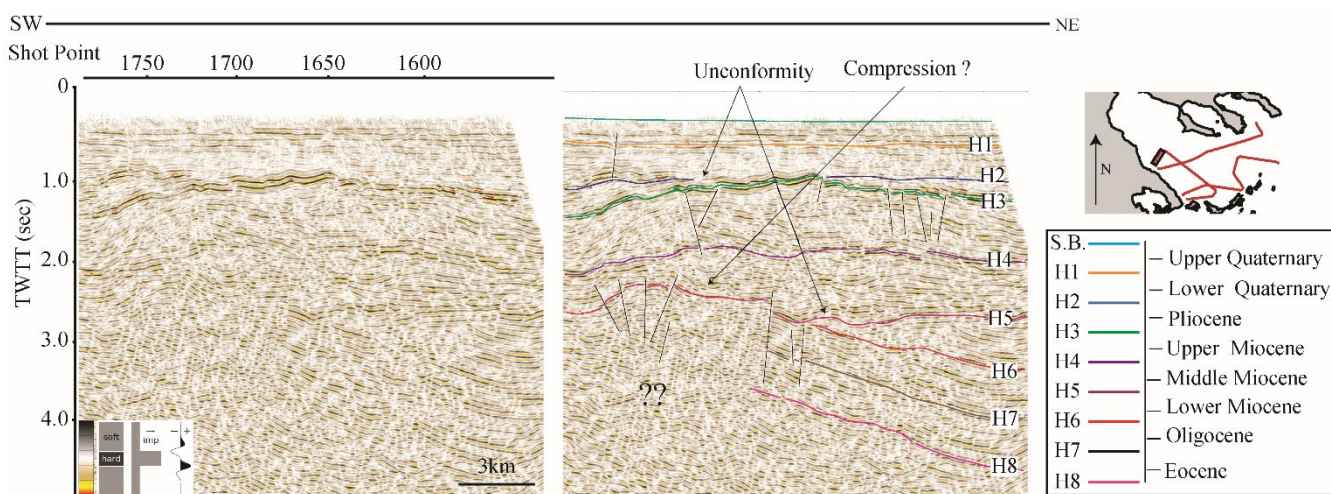


**Figure 5.** Seismic Line NO. Left part: un-interpreted regional seismic profile. Right part: interpreted seismic section with highlighted key horizons and the most prominent tectonic elements.

The N-S transition toward the outer shelf and the continental slope is marked by well-developed clinofolds of SU.1, indicative of shoreline progradation. Characteristically,

a similar configuration is observed in SU.4, indicating the northern fairway as a main source of sedimentation during the Upper Miocene (Figure 6). SU.1–3 are composed of Si facies locally transitioning to Sii, as affected by the syn-depositional tectonism, maintaining an average thickness of 0.3 s that slightly increases to 0.45 s basinwards. The previously reported unconformity between SU.3 and SU.4 (Figure 5) is not observed as the units are conformably developed toward the basinal areas. The thickness of SU.4–7, in contrast to the shallower packages, clearly decreases toward the slope, with mainly Siii facies. The differentiation of their N-S development is probably linked to the activity of the major fault zone clearly expressed in the sea bottom with a WNW strike (FZ 1, Figures 6 and 7). Considering line MN, past the trace of FZ 1 to the SE, only SU.1–4 are mapped (Figure 6). The two uppermost units are characterized by Sii facies transitioning to W toward southeast (Figure 6), where the stratified packages are clearly deformed, illustrating an abrupt change in acoustic coherency and creating a complex, fractured package of reflectors. This alteration in the facies of the units is tentatively linked with a possible, local shear zone affecting clearly SU.1 and the top levels of SU.2, as evidenced by several, minor high-angle faults (Figure 6). Further eastward, the character of the two uppermost units is again dominated by Sii facies, with a more coherent image of stratified reflectors. The presence of bilaterally dipping high-angle faults, and the reverse displacement, along certain faults, of horizon H1 is linked to a possible strike-slip vertical displacement (Figure 6).

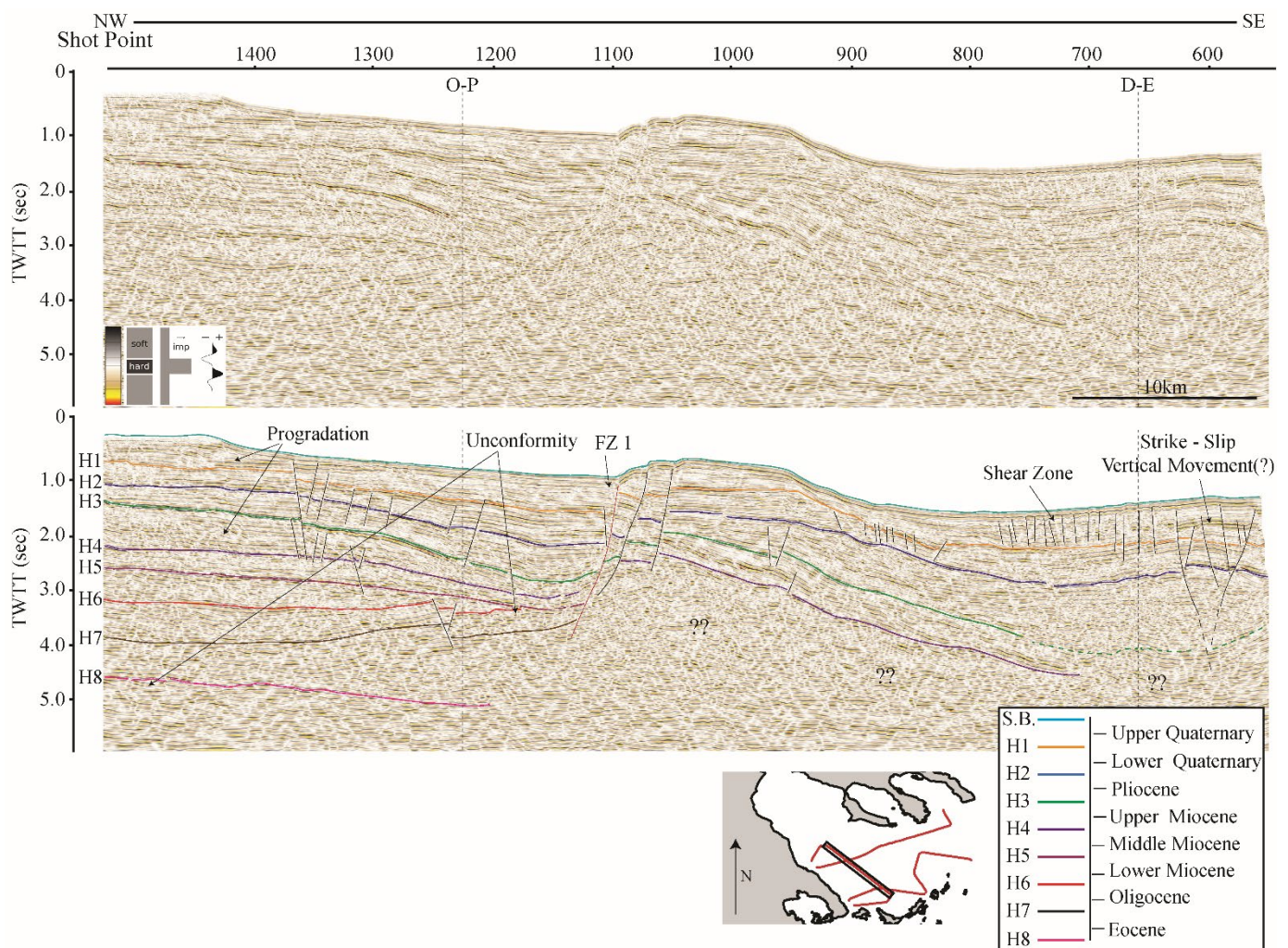


**Figure 6.** Seismic Line MN. Upper part: un-interpreted regional seismic profile. Lower part: interpreted seismic section with highlighted key horizons and the most prominent tectonic elements.

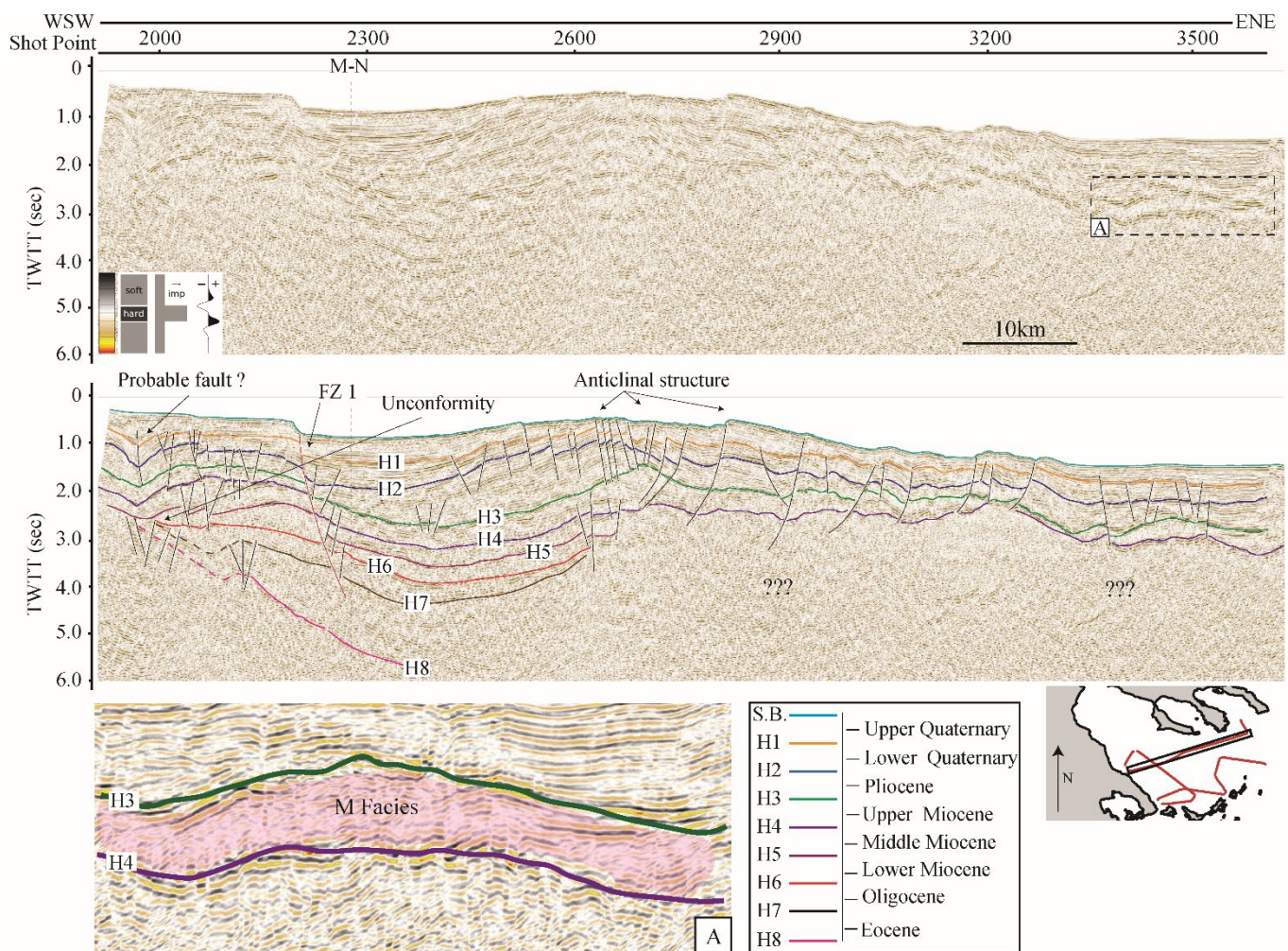


**Figure 7.** Seismic line OP. Upper part: un-interpreted regional seismic profile. Lower part: interpreted seismic section with highlighted key horizons and the most prominent tectonic elements. (A) Differentiated seismic signature of SU.4 characterized by M facies (color-shaded area).

The rest of the picked faults are of moderate-to-high angle, the majority of which affect the shallower formations. The deeper packages (SU.6–7), in accordance with Figure 5, are mapped underlying unconformably SU.5 although their stratigraphical termination is of lower angle (Figure 6). SU.8, composed of Siii facies, is mapped overlying the deeper formations unconformably, and it thickens toward the center of the basin, up until to the point it was able to be mapped as its southern extend is rather incoherent.

The western inner shelf of Thermaikos (Figure 7) indicates high similarity with the configuration of units in Figure 5. SU.1–5 share similar seismic facies (Sii) and time thickness varying from 0.3 to 0.45 s. The western development of the units is affected by the dense tectonism of numerous minor faults and the activity of a probable fault resulting in concave upward geometries (Figure 7). Toward the east, the continuation of FZ 1 as traced in Figure 7 is evident. It is followed by a significant uplift of the units resulting in a local major anticlinal structure (Figures 2 and 7). The displacement of the anticlinal structure (Figure 7) separates the western from the eastern extremity of the area. It also affects the majority of the units in terms of facies and thickness (Sii facies transitioning to Siii). SU.4 characteristically differentiates as it is dominated by M facies (Figure 7A). As in the case of the other two profiles (Figures 5 and 6), SU.6–8 are mapped terminating unconformably under SU.5 (Figure 7), cross-correlating the present unconformity in the extent of Domain A.

#### 4.3.2. Domain B, Western Sporades

Domain B covers the broad area of the western Sporades characterized by the largest depression of the sea bottom, with sea level rising locally to more than 1500 m (Figure 1). The integrated seismic profiles were chosen to be illustrated in joined sections for their most optimal representation (Figures 8 and 9). Due to incoherent, poor image quality and low lateral continuity of the deeper reflectors, only the first three seismic units (up to the top of the Upper Miocene) were effectively mapped.

At the outer southwestern shelf, SU.1–3 are composed of Sii facies terminating at the end of the slope (Figure 8), onlapping uncomfortably over an incoherent package of reflectors characterized by C facies (Figure 9). The basinal regions have the thickest accumulations observed for SU.1–3, as SU.1 reaches a thickness of more than 0.9 s. SU.2–3 are similarly associated with increased average thicknesses of 0.6 and 1.2 s, respectively. The units are dominated by Si, transitioning to Sii facies with an abrupt interruption of W facies (shear zone) expanding toward the western margin of the domain.

Concerning the local tectonism observed, the southwestern margins of the trough have rather steep slopes clearly affected by the action of two major fault zones (Figure 2). The western slope is linked with the presence of FZ 2 with a WNW–ESE strike and high-angle dip with evident normal-drag geometries at the affected units (bent reflectors, Figure 8). The southeastern slope is affected by FZ 3, which as in the case of FZ 2 is associated with an apparent listric-like geometry, characterized by rollover structures and antithetic faults following an ENE–WSW strike (Figure 8).

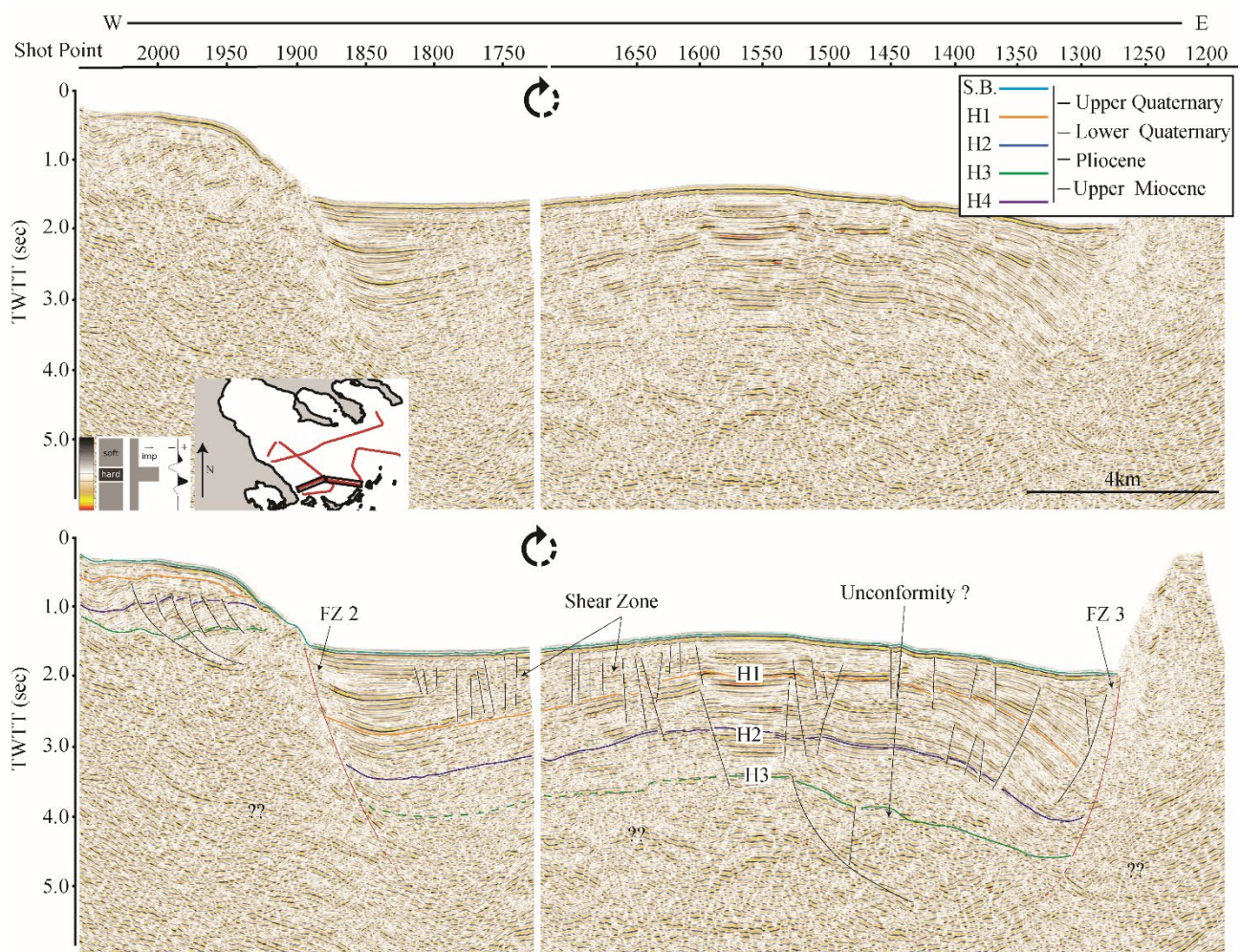


**Figure 8.** Seismic Line EF-DE. Upper part: un-interpreted set of regional seismic profiles. Lower part: interpreted seismic section with highlighted key horizons and the most prominent tectonic elements.

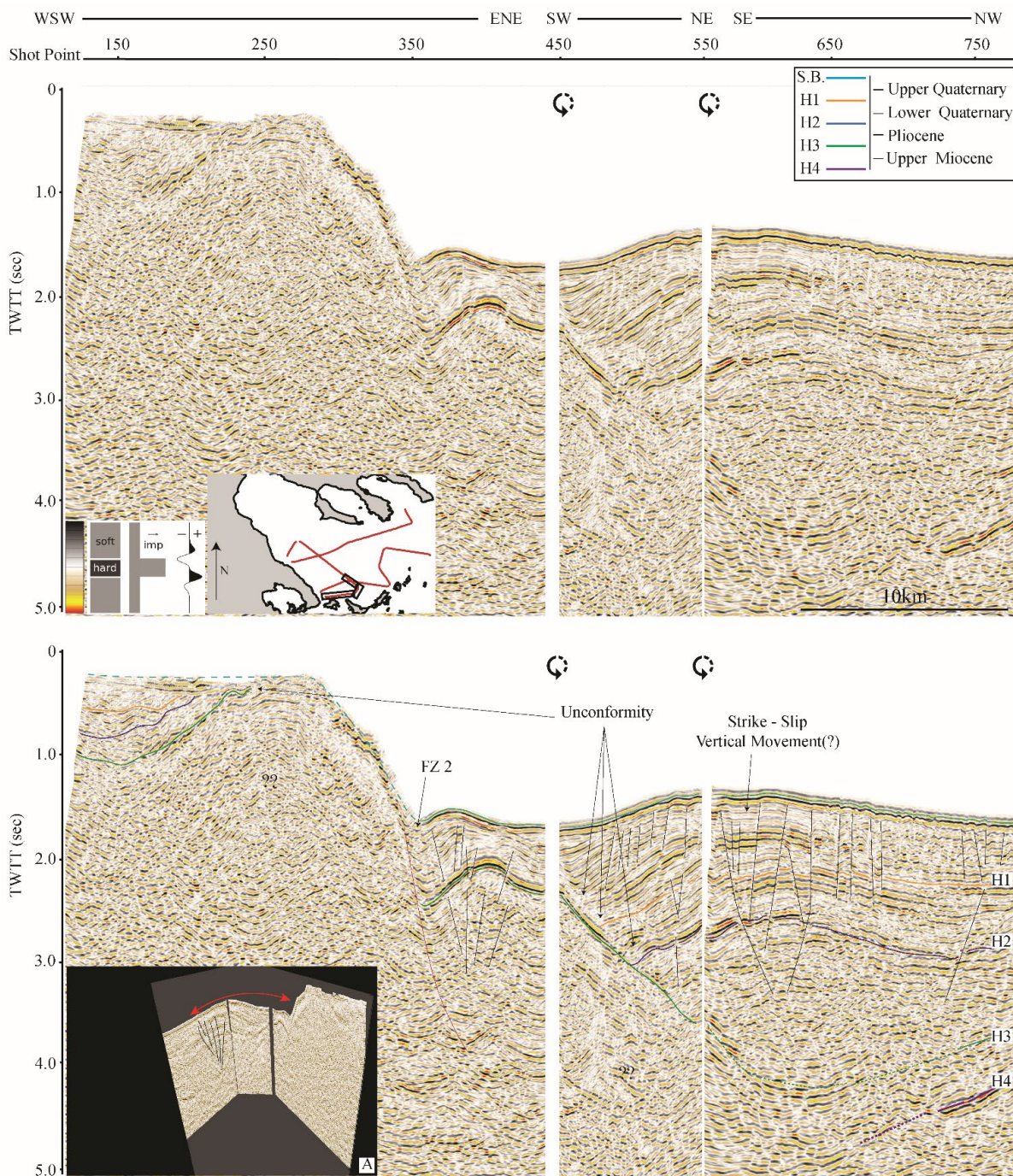


**Figure 9.** Seismic Lines HI, IM, and MN, Upper part: un-interpreted set of regional seismic profiles. Lower part: interpreted seismic sections with highlighted key horizons and the most prominent tectonic elements. (A) 3D perspective of the orientation of the three profiles. The main axis of the strike-slip deformation is tentatively placed parallel to the set of faults in line MN and the local uplift of H3 in line HI.

In Figure 9, a characteristic unconformity is mapped with the termination of SU.1–2 on the surface of H3. This unconformity is related to a significant uplift of the top of SU.4 running parallel to FZ 2 (Figure 8). By observing the trace of the surface of H3 toward the north (line EF in Figure 8), the top of SU.4 is mapped conformably underlying SU.1–3. Considering the fact that the observed anticlinal geometry of H3 in Figure 9 is not continued toward the north suggests a general local reactivation of the southwestern margin of the

NAT tentatively linked to the previously identified, strike-slip component in the southern extremity of line MN (Figures 6 and 9A).

#### 4.3.3. Domain C, Sithonia–Athos Peninsulas

The area covered in this domain follows the eastern end of the previously described anticlinal structure in line OP (Figure 7). The two uppermost seismic units (SU.1–2) share a similar seismic image composed of Si facies with time thickness ranging from 0.25 s near the slope to 0.45 s basinward. The lateral continuation of the formations toward the slope is indicative of SU.1 unconformably overlapping the top of SU.2 (Figure 10). SU.3 is composed of Siii, with a varying thickness of 0.3 s to locally more than 0.65 s. As mentioned, SU.4 is considerably differentiated in terms of acoustic image, dominated by M facies. The local character of the unit is observed with the presence of a chaotic, transparent package of internal reflectors bounded by high-amplitude reflectors (H3 and H4). The thickness of the unit ranges from 0.27 to 0.36 s following an updoming geometry with evident tectonism.

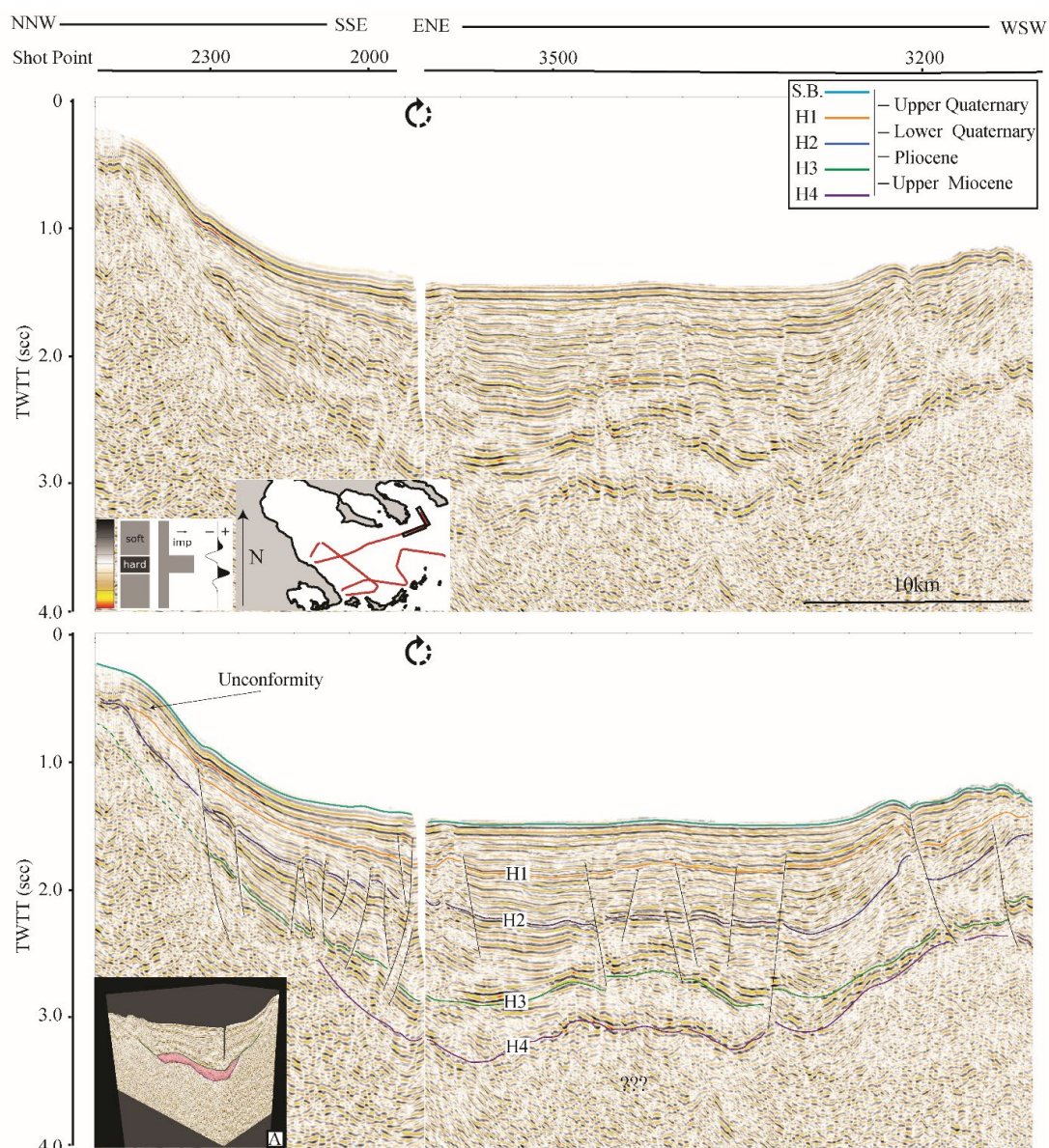


**Figure 10.** Seismic Line PR-OP. Upper part: un-interpreted set of regional seismic profiles. Lower part: interpreted seismic section with highlighted key horizons and the most prominent tectonic elements. (A) 3D perspective of the orientation of the three profiles, with SU.4 highlighted.

#### 4.3.4. Domain D, Eastern Sporades

Domain D covers the outer shelf of the eastern Sporades and part of the deeper central region of the NAT. The seismic mapping process was applicable only down to SU.4 due to the disturbed quality of the deeper reflectors. In the western extremity of the domain (Figure 11), SU.1–2 are dominated by rather thick (0.7 to 0.9 s and 0.45 to 0.8 s, respectively) Si facies. SU.3 is composed of Sii facies (0.4 s) with locally observed transparent reflections. SU.4 is characterized by Siii facies illustrating a decreasing thickness toward the west (0.2 s). The faults picked are mainly of high angle and large extent as they affect all the thick packages of the aforementioned units. Near the margin, the reflection quality is clearly diminished, probably due to the presence of the NW dipping fault zone (FZ 3) interpreted to be the continuum of the same displacement observed in Domain B (Figure 8).

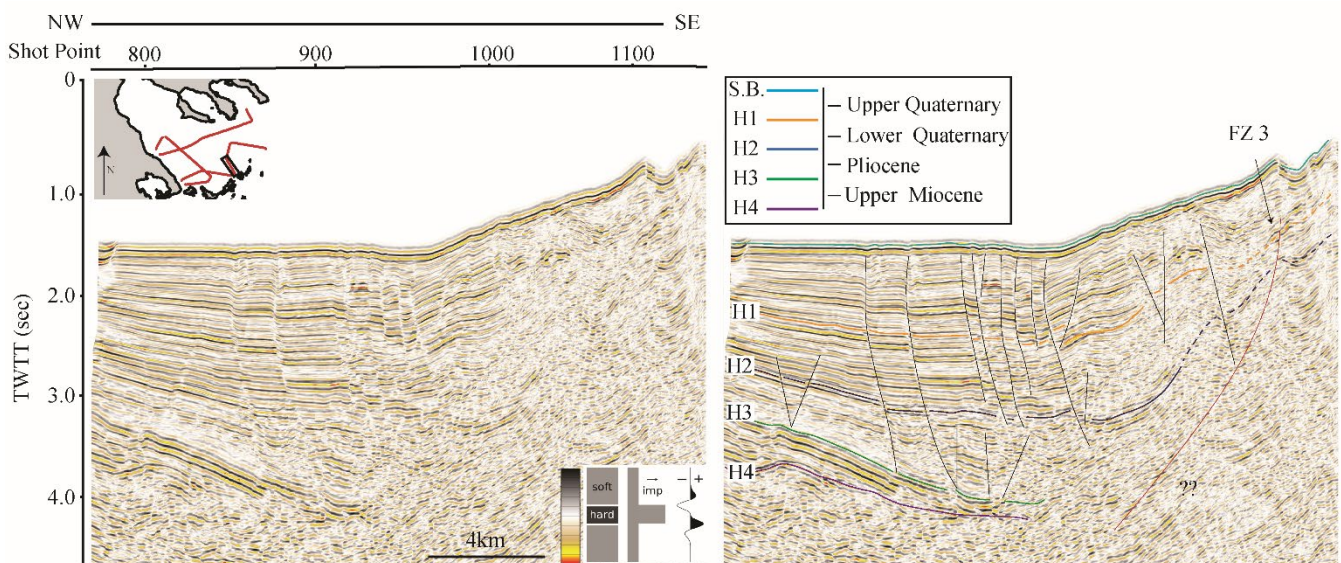


**Figure 11.** Seismic Line CD. Left part: un-interpreted set of regional seismic profiles. Right part: interpreted seismic section with highlighted key horizons and the most prominent tectonic elements.

Toward the central regions (Figure 12), the same units form a local graben with numerous local faults reaching down to SU.3. SU.1–2 are dominated by Si and Sii facies (0.4 and 0.55 s respectively), while SU.3, composed of Siii, is thinner near the western end, gradually increasing toward the east (0.6 s). Near the eastern limit (Figure 13), the acoustic image is rather incoherent, as the prominent reflector continuity is disturbed with local transparent and chaotic reflectors of poor lateral extent. SU.1 has an average thickness of 0.65 s and composed of Sii transitioning to Siii facies. SU.2–3 are of Siii facies (0.25–0.3 s, respectively). Toward the continental slope, the units transition to C facies, due to the presence of two apparent bilateral faults, while the same units are observed displaying Siii facies, onlapping over the probable NE continuation of FZ 3 (Figure 13).

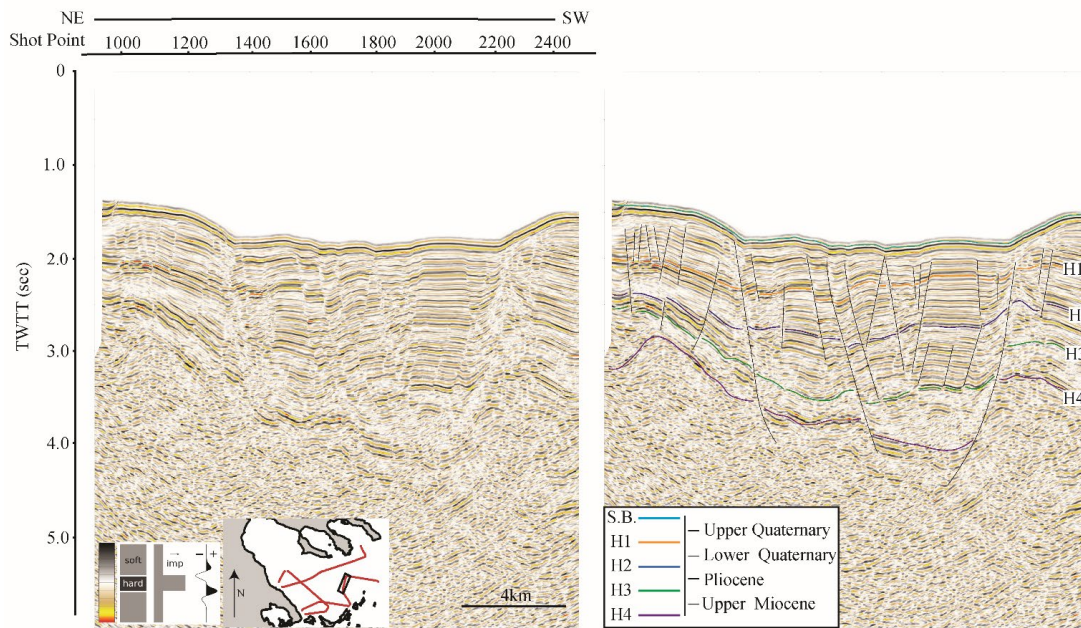


**Figure 12.** Seismic Line BC. Left part: un-interpreted set of regional seismic profiles. Right part: interpreted seismic section with highlighted key horizons and the most prominent tectonic elements.

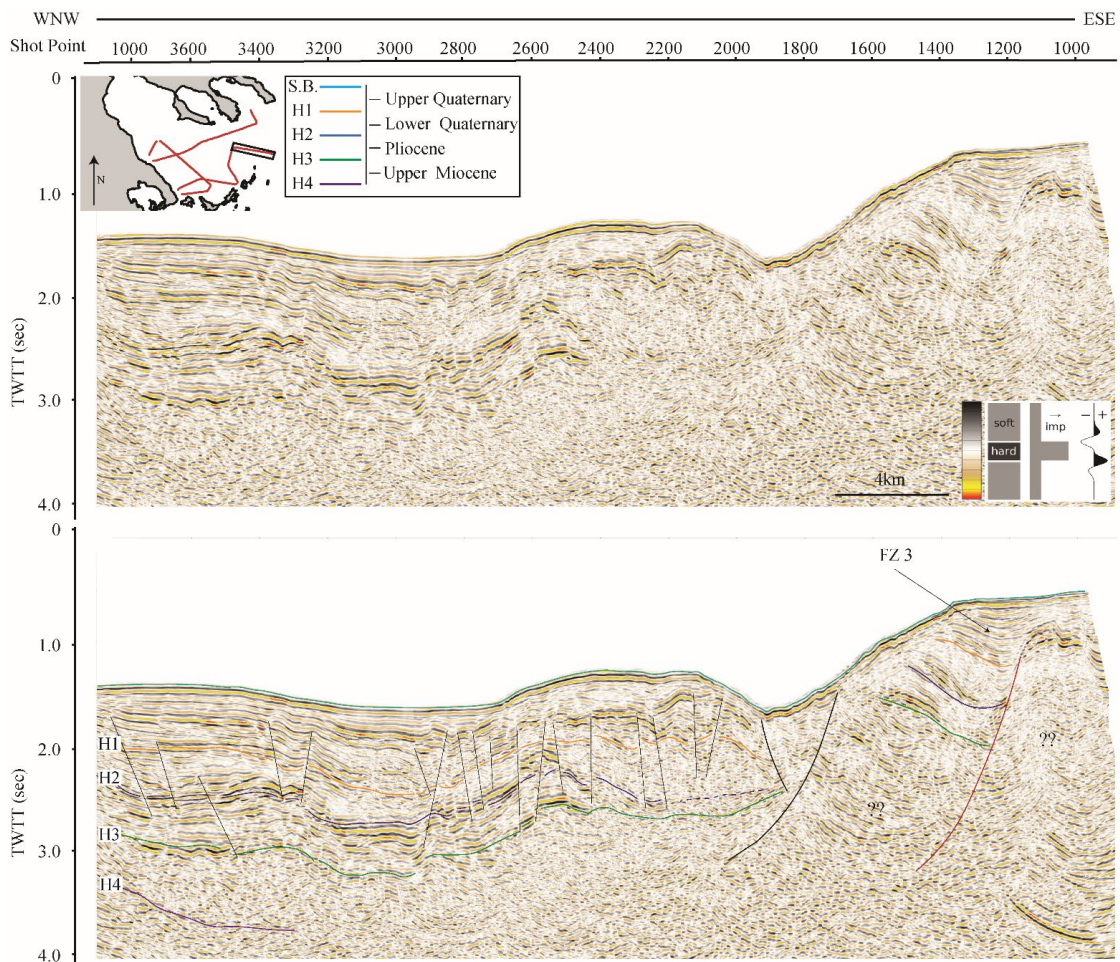


**Figure 13.** Seismic Line AB. Upper part: un-interpreted set of regional seismic profiles. Lower part: interpreted seismic section with highlighted key horizons and the most prominent tectonic elements.

## 5. Discussion

The North Aegean Sea is today dominated by the overwhelming tectonics of the North Aegean Trough. However, its margin appears to have hosted important geotectonic events that culminated in thick autochthonous sedimentary sequences since the Paleogene, as established in this study on the basis of deep penetrating seismic profiles.

### 5.1. Paleogene

The westernmost region of the NAT is thought to have been affected by tectonic processes linked to the exhumation of the Southern Rhodope Complex during Paleogene [52,53], leading to the creation of accommodation space, resulting in thick sediment accumulations. Onshore wells in the Kassandra Peninsula (Figure 3) recovered thick clastic sequences that gradually pass to the north to a bathyal-shallow neritic condition of the Upper Eocene–Oligocene age [54]. In the northwestern Thermaikos offshore wells, the chronostratigraphic framework of Faugères and Robert [39] and Lalechos and Savoyat [40] differ with regard to the top of the Paleogene. The first authors proposed a Neogene section of 3500 m thick, whereas the second study proposed a thickness of 2600 m, attributing the deeper series identified in the wells to the Upper Eocene and Oligocene age. The acoustic character of the two deeper units (SU.7 and SU.8) identified in the present study (Figures 5–7) and their tracing in the outer shelf of Thermaikos favored the interpretation of Lalechos and Savoyat [40] and suggested the prevalence of marine conditions during Paleogene (Figure 14A,B), as indicated by the reflection configuration of the units. Moreover, SU.8's fan architecture packages (Figures 6 and 7), plus laterally discontinuous reflectors, possibly suggest a middle-to-outer submarine fan environment. SU.7 is defined between unconformities cutting toplapping underlying reflectors. Toward the Kassandra Peninsula, the Eocene–Oligocene thickens in agreement with the PO-1 drillhole (Figure 3) that recovered the thickest Eocene and Oligocene. We envision a possible intermittent marine corridor pointing through the Axios fault valley to the north toward Paratethys. The obscure termination of H8 to H6 reflectors in the outer periphery of the Thermaikos slope (Figure 7) extending south to the Sporades Islands suggests intense tectonic processes. Although it has been suggested that Paleogene marine conditions extended to the west of the Olympos–Ossa–Pelion range [36], any evidence of marine sedimentary sequences in the periphery of the NAT is obscured by tectonism.

### 5.2. Lower-Middle Miocene

As shown in Figure 3, all Thermaikos wells recovered thick Miocene sequences overlying Oligocene sediments. In particular, the offshore middle shelf well TH-A1 retrieved an over 250 m thick basal conglomerate over marine Oligocene sediments. The extent of SU.6 in Thermaikos (Figures 5–7) is enclosed by well-defined unconformities developed over toplap reflector terminations. Our H6 and H5 reflectors correlate well with the analysis of IFP [38] (Figure 4) that included several drillholes along seismic profiles placing Lower Miocene series, unconformably underlying the shallower units.

The overlying Middle Miocene packages (SU.5) display an unconformable development over the deeper units, as evidenced by the angular development of H5 across the outer Thermaikos (Figures 5–7). The enhanced thickness of the unit, as observed at the western margin of the trough (WSW end in line OP, Figure 7), is attributed to the syn-depositional tectonic activity of a probable fault with an NW apparent strike, as well as the development of numerous normal faults of similar strike deforming SU.5. We further emphasize the development of thinner SU.5 packages characterized by the absence of tectonic activity toward the eastern continuation of the unit in line OP (Figure 7). This is thought to be due to a relatively slower rate of subsidence at the eastern margin of the basin (toward the Kassandra Peninsula) (Figure 14D). We further observe the abrupt termination of pre-Upper Miocene reflectors against the bottom surface of SU.5, extending all along the outer Thermaikos slope.

### 5.3. Upper Miocene

In the Upper Miocene (SU.4), we observe clear evidence of overall extensional differential subsidence all along the North Aegean Trough margin. Lateral and vertical sedimentary facies alterations are observed, attributed mostly to resedimentation processes related to tectonics. In the western NAT (Figure 14E), we observe characteristic progradation packages (Figure 6) feeding the southern depocenter of western Sporades, while the dense tectonism affecting SU.4 in the western margin of the trough seems to associate with the predominant Upper Miocene WNW–ESE tensional direction as reported by Mercier et al. [55]. Toward the eastern Sporades, (Figures 11–13), the associated packages are thinner, possibly resulting from lower subsidence rates. The sub-basins, south of the Sigitikos Gulf, display a different evolution, as evidenced by the clear differentiation of SU.4's seismic facies (Figures 7A and 10).

SU.4 in Domain C is characteristically enclosed within top and bottom horizons displaying high acoustic amplitude, bounding a package of chaotic, transparent reflectors (Figures 7A and 10). Additionally, the geometry of the unit is indicative of gentle folding and small-scale general up-doming. In compliance with the salt delineation criteria of Jackson and Hudec [56], the seismic image of the unit can be attributed to evaporite salt deposition. By applying the Messinian Salinity Crisis nomenclature as proposed by Lofi et al. [57] and Roveri et al. [58], the acoustic character of reflector H3, from west to east, can be correlated to the TS/TES (top or top erosional surface). Accordingly, the marker horizon H4 corresponds to the bottom erosional surface (BES) enclosing the transparent facies that is attributed to the mobile unit. This interpretation correlates to the well-established West Mediterranean trilogy of Montadert et al. [59] and to a lesser extent to the similar units identified in the deep Eastern Mediterranean [60] and also in the North Ionian Sea Basin [61]. South of the Chalkidiki peninsula, Mascle and Martin [17] identified diapir-like structures indicative of evaporitic Messinian series, in agreement with Ferentinos' [62] earlier identification of salt structures across the NAT. Lalechos and Savoyat [40] proposed that the extent of evaporitic accumulations from the northeastern basins (Prinos-Nestos) terminated in the above-mentioned region. In this vicinity also, Needham et al. [63] identified a high-velocity layer.

The offshore wells in Thermaikos (Figure 3) did not report the presence of evaporitic formations at the top of the Upper Miocene. This is justified by the prograding clinoform packages identified, suggesting the overwhelming dominance of fluvial-coastal zone progradations in that region (Figure 6).

#### Implications of the NAF's Deformation Timing

In the North Aegean Trough, north of western Sporades islands, the Upper Miocene (SU.4) is strongly tectonized. The bottom surface of the unit (H4) is poorly traced due to incoherent seismic images in lines HI and IM (Figure 9). This is attributed to tectonic deformation. The top surface of SU.4 is strongly uplifted, terminating with a characteristic anticlinal geometry at the fault plane of the marginal fault zone (FZ 2) (Figure 9). In contrast, the level of the same surface (horizon H3), in the sub-parallel line, EF (Figures 1 and 8) is traced under a sub-parallel series of conformable overlying, units (SU.1–3).

The shallower development of H3 at the southwestern regions of the trough (line HI, Figure 9) in comparison to line EF (Figure 8) displays a distinct unconformity with the younger units that generally downlap over its surface (horizons H 1–2 in line IM, Figure 9). This unconformity complies with the absence of SU.1–3 in line HI (Figure 9). In the region, we observe the reverse displacement of the shallower horizons (H1 and H2) among a set of bilaterally dipping faults, as shown in the southeastern end of line MN (Figures 6 and 9). This implies a compressional reactivation of the units along the broader region of western Sporades (Figure 2), within the area of strike-slip vertical fault zones, as reported by Papanikolaou et al. [25].

The deformation of the top of unit SU.4, assigned to the Upper Miocene of the NAT, further provides evidence that the timing of the NAF's propagation in the North Aegean

occurred at the later stages of the Miocene, as originally proposed by Armijo et al. [4], eventually reaching the Gulf of Corinth at around 1 Ma [64,65].

#### 5.4. Pliocene-Quaternary

The Pliocene-Quaternary is characterized by increased sediment accumulation rates especially in the eastern and southern sections (Figures 6 and 7) of the western NAT. This is due to the increase in the accommodation space as a result of drastic subsidence coupled with failures on the upper slope and shelf, resulting in gravity flows transporting sediments into the deeper parts of the basin. During Pliocene, the increased thickness of the associated packages (SU.3) is mostly observed toward the east, in line OP (Figure 7) and toward the south in line MN (Figure 6). This is attributed to the syn-rift depositional phase characterized by higher rates of subsidence (Figure 14F). This increase in the accommodation space is probably due to the tectonic reactivation of the southwestern marginal faults (FZ 2 and FZ 3, Figures 8, 9, and 13) attributed to the westward propagation of the NAF. The major anticlinal structure extending in the northern margin of the NAT seems to be connected to the latter stages of the Pliocene. The syn-depositional activity of FZ 1 is manifested along the western end of the trough characterized also by higher sediment accumulation rates (Figure 7).

The Upper and Lower Quaternary packages (SU.1–2) suggest a steady, marine depositional setting (mainly characterized by Si and Sii facies) locally affected by the active tectonics in the trough (mapped faults and W facies interruptions, Figures 6 and 8). The numerous faults observed at the limbs and hinge of the anticline structure in line OP (Figure 7) and the growth of SU.1–2 at the plane of FZ 1 (Figures 2, 6, and 7) suggest the progress of tectonic deformation to the northern margins of the NAT as originated by the NAF's activity.

Along the N–S direction of Domain A, the shallowest unit (SU.1) is associated with a characteristic clinoform geometry (Figure 6), the inflection breakpoints of which are linked to seaward reaches of the coastal zone. Generally, these display an aggradation–progradation stacking pattern in the Upper Quaternary as postulated by Brooks and Ferentinos [20] and Lykousis [66]. The two units are heavily affected by numerous minor faults with an NW apparent strike, something that agrees with the prevalence of an NE–SW extensional regime during Lower Pleistocene Mercier et al. [55] and the proposition of its most recent transition toward a northern direction [55,67,68].

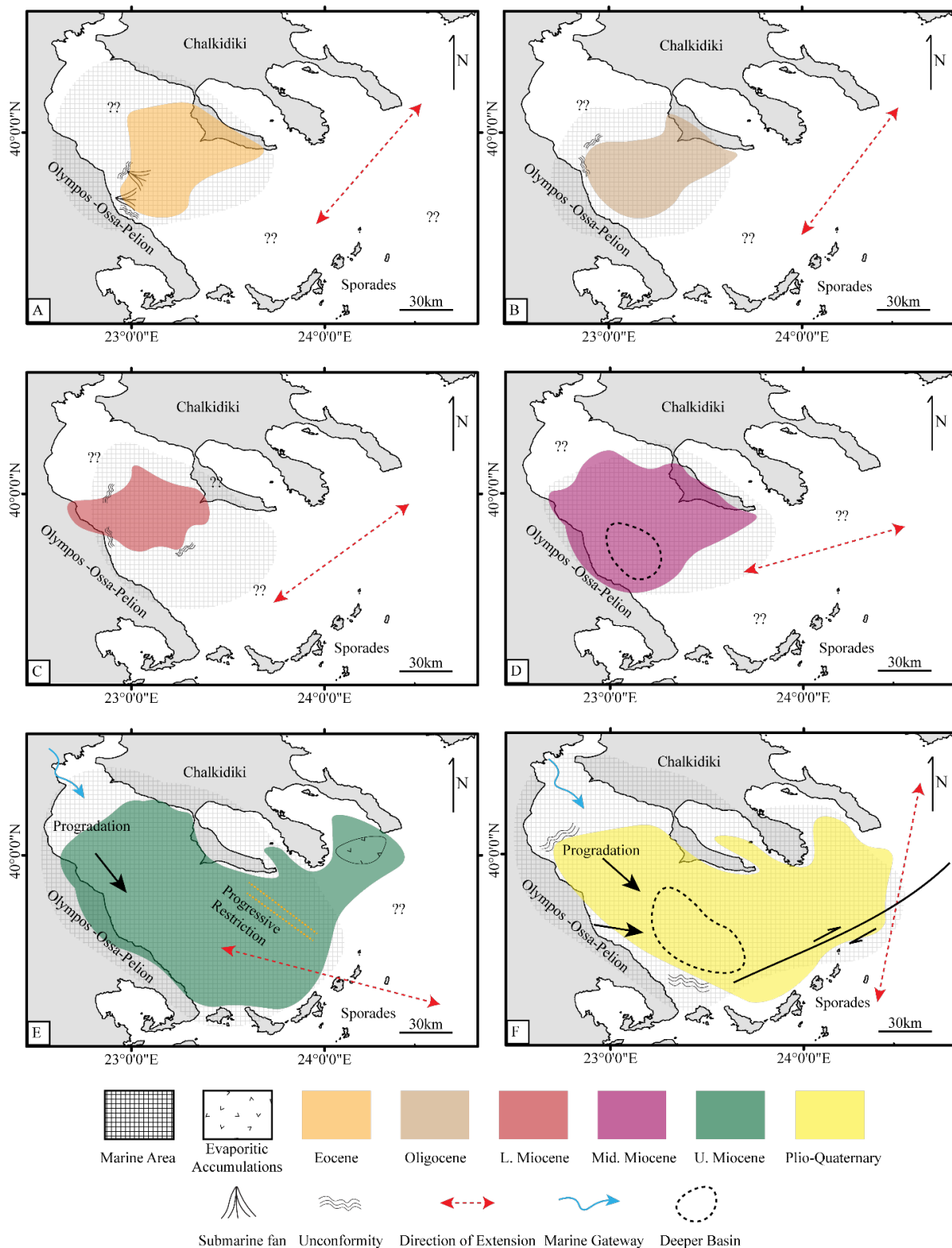


**Figure 14.** Schematic maps of the paleogeographic basin reconstruction during the various stratigraphic intervals: (A) Eocene, (B) Oligocene, (C) L. Miocene, (D) M. Miocene, (E) U. Miocene, and (F) Pliocene-Quaternary. The extension of the coverage is constrained by the mapping of each unit in the seismic sections and their correlative extent as directed by the neighboring wells, where applicable. Extensional direction is based on the mapped faults as correlated with Brun and Sokoutis [52,53] for Paleogene–Early Miocene, Mercier et al. [55] for Upper Miocene, and Mercier et al. [55], Kahle et al. [67], and Le Pichon et al. [68] for Pliocene and Quaternary.

## 6. Conclusions

The seismic stratigraphic synthesis of the western North Aegean Trough was achieved through the integration of deep penetration 2D multichannel seismic data. We conclude the following:

- A trough-shaped roughly N–S-trending basin extending from northern mainland Greece to the outer Thermaikos slope formed as a result of persistent NE–SW extension since early Paleogene.
- This Axios basin formed to the north of the Upper Cretaceous Vardar Ocean suture zone that was confined in the outer periphery of the NAT that was elevated.
- The southern extents of the Axios basin remained continuously marine since the Eocene, with possible intermittent marine connections to Paratethys at Cenozoic Sea level highstands and possibly connecting to the Mesohellenic Basin.
- The sedimentary stratigraphic record, as reflected by seismic facies observed in the western NAT, is in good agreement with the directions of extension proposed in previous studies: (a) the NE–SW extension observed in late Paleogene–early Miocene sections on land, (b) a gradual shift toward a WNW–ESE extensional regime during the Miocene, and (c) a consequent gradual prevalence of an NNE–SSW extension in the Pliocene–Quaternary.
- The kinematic timing of the North Anatolian Fault propagation in the NAT is outlined. The mapping of compressional deformation in the Upper Miocene–Early Pliocene in the western Sporades constrains the arrival of the NAF, transitioning to the north during the Quaternary.
- The likely presence of Messinian evaporites, including salt, is postulated in the western regions of the NAT, south of the Chalkidiki Peninsula as established on the basis of BES and TES.

**Author Contributions:** Conceptualization: G.A. and A.V.; Methodology: A.V.; Software: A.V. and G.A.; Writing—original draft preparation: A.V. and G.A.; Writing—review and editing: A.V. and G.A. All authors have read and agreed to the published version of the manuscript.

**Funding:** This research received no external funding.

**Institutional Review Board Statement:** Not applicable.

**Informed Consent Statement:** Not applicable.

**Data Availability Statement:** Data that support the findings of this study are available from the corresponding author upon reasonable request.

**Acknowledgments:** The authors would like to express their gratitude to Alferd Hirn, Institut de Physique du Globe, for providing the seismic reflection dataset. We want to thank DownUnder Geosolutions for providing an academic license of DUG Insight. We gratefully acknowledge David J.W. Piper for his thorough review. The academic editor and the two anonymous reviewers are acknowledged for their useful and constructive comments.

**Conflicts of Interest:** The authors declare no conflict of interest.

## References

1. Jackson, J. Active Tectonics of the Aegean Region. *Annu. Rev. Earth Planet. Sci.* **1994**, *22*, 239–271. [[CrossRef](#)]
2. Le Pichon, X.; Şengör, A.M.C.; Kende, J.; İmren, C.; Henry, P.; Grall, C.; Karabulut, H. Propagation of a Strike-Slip Plate Boundary within an Extensional Environment: The Westward Propagation of the North Anatolian Fault. *Can. J. Earth Sci.* **2016**, *53*, 1416–1439. [[CrossRef](#)]
3. Reilinger, R.E.; McClusky, S.C.; Oral, M.B.; King, R.W.; Toksoz, M.N.; Barka, A.A.; Kinik, I.; Lenk, O.; Sanli, I. Global Positioning System Measurements of Present-Day Crustal Movements in the Arabia-Africa-Eurasia Plate Collision Zone. *J. Geophys. Res. Solid Earth* **1997**, *102*, 9983–9999. [[CrossRef](#)]
4. Armijo, R.; Meyer, B.; Hubert, A.; Barka, A. Westward Propagation of the North Anatolian Fault into the Northern Aegean: Timing and Kinematics. *Geology* **1999**, *27*, 267. [[CrossRef](#)]
5. Savostin, L.A.; Sibuet, J.-C.; Zonenshain, L.P.; Le Pichon, X.; Roulet, M.-J. Kinematic Evolution of the Tethys Belt from the Atlantic Ocean to the Pamirs since the Triassic. *Tectonophysics* **1986**, *123*, 1–35. [[CrossRef](#)]

6. Royden, L.H. Evolution of Retreating Subduction Boundaries Formed during Continental Collision. *Tectonics* **1993**, *12*, 629–638. [[CrossRef](#)]
7. Jacobshagen, V. Orogenic evolution of the Hellenides: New aspects. In *Active Continental Margins—Present and Past*; Springer: Berlin, Heidelberg, 1994; pp. 249–256.
8. Dinter, D.A. Late Cenozoic Extension of the Alpine Collisional Orogen, Northeastern Greece: Origin of the North Aegean Basin. *Geol. Soc. Am. Bull.* **1998**, *110*, 1208–1230. [[CrossRef](#)]
9. Walcott, C.; White, S. Constraints on the Kinematics of Post-Orogenic Extension Imposed by Stretching Lineations in the Aegean Region. *Tectonophysics* **1998**, *298*, 155–175. [[CrossRef](#)]
10. Ring, U.; Gessner, K.; Güngör, T.; Passchier, C.W. The Menderes Massif of Western Turkey and the Cycladic Massif in the Aegean—Do They Really Correlate? *J. Geol. Soc.* **1999**, *156*, 3–6. [[CrossRef](#)]
11. Papanikolaou, D.; Alexandri, M.; Nomikou, P.; Ballas, D. Morphotectonic Structure of the Western Part of the North Aegean Basin Based on Swath Bathymetry. *Mar. Geol.* **2002**, *190*, 465–492. [[CrossRef](#)]
12. Taymaz, T.; Yilmaz, Y.; Dilek, Y. The Geodynamics of the Aegean and Anatolia: Introduction. *Geol. Soc. Lond. Spec. Publ.* **2007**, *291*, 1–16. [[CrossRef](#)]
13. McKenzie, D. Active Tectonics of the Alpine–Himalayan Belt: The Aegean Sea and Surrounding Regions. *Geophys. J. Int.* **1978**, *55*, 217–254. [[CrossRef](#)]
14. Faccenna, C.; Bellier, O.; Martinod, J.; Piromallo, C.; Regard, V. Slab Detachment beneath Eastern Anatolia: A Possible Cause for the Formation of the North Anatolian Fault. *Earth Planet. Sci. Lett.* **2006**, *242*, 85–97. [[CrossRef](#)]
15. Brun, J.-P.; Sokoutis, D. 45 m.y. of Aegean Crust and Mantle Flow Driven by Trench Retreat. *Geology* **2010**, *38*, 815–818. [[CrossRef](#)]
16. Brun, J.-P.; Faccenna, C.; Gueydan, F.; Sokoutis, D.; Philippon, M.; Kydonakis, K.; Gorini, C. The Two-Stage Aegean Extension, from Localized to Distributed, a Result of Slab Rollback Acceleration. *Can. J. Earth Sci.* **2016**, *53*, 1142–1157. [[CrossRef](#)]
17. Mascle, J.; Martin, L. Shallow Structure and Recent Evolution of the Aegean Sea: A Synthesis Based on Continuous Reflection Profiles. *Mar. Geol.* **1990**, *94*, 271–299. [[CrossRef](#)]
18. Sakellariou, D.; Rousakis, G.; Morfis, I.; Panagiotopoulos, I.; Ioakim, C.; Trikalinou, G.; Tsampouraki-Kraounaki, K.; Kranis, H.; Karageorgis, A.P. Deformation and Kinematics at the Termination of the North Anatolian Fault: The North Aegean Trough. In Proceedings of the 9th International INQUA Meeting on Paleoseismology, Active Tectonics and Archeoseismology (PATA), Possidi, Greece, 25–27 June 2018.
19. Sakellariou, D.; Tsampouraki-Kraounaki, K. Offshore Faulting in the Aegean Sea: A Synthesis Based on Bathymetric and Seismic Profiling Data. *Bull. Geol. Soc. Greece* **2017**, *50*, 134. [[CrossRef](#)]
20. Brooks, M.; Ferentinos, G. Structure and Evolution of the Sporadhes Basin of the North Aegean Trough, Northern Aegean Sea. *Tectonophysics* **1980**, *68*, 15–30. [[CrossRef](#)]
21. Ferentinos, G.; Brooks, M.; Collins, M. Gravity-Induced Deformation On the North Flank and Floor of the Sporadhes Basin of the North Aegean Sea Trough. *Mar. Geol.* **1981**, *44*, 289–302. [[CrossRef](#)]
22. Bulut, F.; Özener, H.; Doğru, A.; Aktuğ, B.; Yaltrak, C. Structural Setting along the Western North Anatolian Fault and Its Influence on the 2014 North Aegean Earthquake (Mw 6.9). *Tectonophysics* **2018**, *745*, 382–394. [[CrossRef](#)]
23. Kiratzi, A.; Louvari, E. Focal Mechanisms of Shallow Earthquakes in the Aegean Sea and the Surrounding Lands Determined by Waveform Modelling: A New Database. *J. Geodyn.* **2003**, *36*, 251–274. [[CrossRef](#)]
24. Ganas, A.; Drakatos, G.; Pavlides, S.B.; Stavrakakis, G.N.; Ziazia, M.; Sokos, E.; Karastathis, V.K. The 2001 Mw = 6.4 Skyros Earthquake, Conjugate Strike-Slip Faulting and Spatial Variation in Stress within the Central Aegean Sea. *J. Geodyn.* **2005**, *39*, 61–77. [[CrossRef](#)]
25. Papanikolaou, D.; Alexandri, M.; Nomikou, P. Active Faulting in the North Aegean Basin. *Spec. Pap. Geol. Soc. Am.* **2006**, *409*, 189–209. [[CrossRef](#)]
26. Laigle, M.; Hirn, A.; Sachpazi, M.; Roussos, N. North Aegean Crustal Deformation: An Active Fault Imaged to 10 Km Depth by Reflection Seismic Data. *Geology* **2000**, *28*, 71–74. [[CrossRef](#)]
27. Koukouvelas, I.K.; Aydin, A. Fault Structure and Related Basins of the North Aegean Sea and Its Surroundings. *Tectonics* **2002**, *21*, 1–17. [[CrossRef](#)]
28. Müller, M.D.; Geiger, A.; Kahle, H.-G.; Veis, G.; Billiris, H.; Paradissis, D.; Felekis, S. Velocity and Deformation Fields in the North Aegean Domain, Greece, and Implications for Fault Kinematics, Derived from GPS Data 1993–2009. *Tectonophysics* **2013**, *597–598*, 34–49. [[CrossRef](#)]
29. Lazos, I.; Sboras, S.; Pikridas, C.; Pavlides, S.; Chatzipetros, A. Geodetic Analysis of the Tectonic Crustal Deformation Pattern in the North Aegean Sea, Greece. *Mediterr. Geosci. Rev.* **2021**, *3*, 79–94. [[CrossRef](#)]
30. Floyd, M.A.; Billiris, H.; Paradissis, D.; Veis, G.; Avallone, A.; Briole, P.; McClusky, S.; Nocquet, J.-M.; Palamartchouk, K.; Parsons, B.; et al. A New Velocity Field for Greece: Implications for the Kinematics and Dynamics of the Aegean. *J. Geophys. Res.* **2010**, *115*, B10403. [[CrossRef](#)]
31. McNeill, L.C.; Mille, A.; Minshull, T.A.; Bull, J.M.; Kenyon, N.H.; Ivanov, M. Extension of the North Anatolian Fault into the North Aegean Trough: Evidence for Transtension, Strain Partitioning, and Analogues for Sea of Marmara Basin Models. *Tectonics* **2004**, *23*, 1–12. [[CrossRef](#)]
32. Sakellariou, D.; Tsampouraki-Kraounaki, K. Plio-Quaternary Extension and Strike-Slip Tectonics in the Aegean. In *Transform Plate Boundaries and Fracture Zones*; Elsevier: Amsterdam, The Netherlands, 2019; pp. 339–374, ISBN 9780128120644.

33. Lybérís, N. Tectonic Evolution of the North Aegean Trough. *Geol. Soc. Lond. Spec. Publ.* **1984**, *17*, 709–725. [[CrossRef](#)]
34. Roussos, N.; Lyssimachou, T. Structure of the Central North Aegean Trough: An Active Strike-Slip Deformation Zone. *Basin Res.* **1991**, *3*, 37–46. [[CrossRef](#)]
35. Ferentinos, G.; Georgiou, N.; Christodoulou, D.; Geraga, M.; Papatheodorou, G. Propagation and Termination of a Strike Slip Fault in an Extensional Domain: The Westward Growth of the North Anatolian Fault into the Aegean Sea. *Tectonophysics* **2018**, *745*, 183–195. [[CrossRef](#)]
36. Roussos, N. Stratigraphy and Paleogeographic Evolution of Palaeocene Molassic Basins of N. Aegean. *Bull. Geol. Soc. Greece* **1994**, *XXX*, 275–294.
37. Aidona, E.; Kondopoulou, D.; Scholger, R.; Georgakopoulos, A.; Vafeidis, A. Palaeomagnetic Investigations of Sediments Cores from Axios Zone (N. Greece): Implications of Low Inclinations in the Aegean. *eEarth* **2008**, *3*, 7–18. [[CrossRef](#)]
38. IFP. *Rapport Sur Le Bassin de Thessalie, Grece. Unpubl.*; 1965.
39. Faugères, L.; Robert, C.M. Etude Sédimentologique et Minéralogique de Deux Forages Du Golfe Thermaique (Mer Egée). *Géologie Méditerranéenne* **1976**, *3*, 209–218. [[CrossRef](#)]
40. Lalechos, N.; Savoyat, E. La Sedimentation Neogene Dans Le Fosse Nord Egeen. *VI Colloquium Geol. Aegean Reg.* **1979**, *2*, 591–603.
41. Beniést, A.; Brun, J.P.; Gorini, C.; Crombez, V.; Deschamps, R.; Hamon, Y.; Smit, J. Interaction between Trench Retreat and Anatolian Escape as Recorded by Neogene Basins in the Northern Aegean Sea. *Mar. Pet. Geol.* **2016**, *77*, 30–42. [[CrossRef](#)]
42. Proedrou, P.; Sidiropoulos, T. Prinos Field—Greece Aegean Basin. *Struct. Traps VI AAPG Spec. Vol.* **1992**, 275–291.
43. Proedrou, P.; Papaconstantinou, M.C. Prinos Basin—A Model for Oil Exploration. *Bull. Geol. Soc. Greece* **2004**, *36*, 327–333. [[CrossRef](#)]
44. Snel, E.; Mărunțeanu, M.; Meulenkamp, J.E. Calcareous Nannofossil Biostratigraphy and Magnetostratigraphy of the Upper Miocene and Lower Pliocene of the Northern Aegean (Orphanic Gulf-Strimon Basin Areas), Greece. *Palaeogeogr. Palaeoclimatol. Palaeoecol.* **2006**, *238*, 125–150. [[CrossRef](#)]
45. Karakitsios, V.; Cornée, J.-J.; Tsourou, T.; Moissette, P.; Kontakiotis, G.; Agiadi, K.; Manoutsoglou, E.; Triantaphyllou, M.; Koskeridou, E.; Drinia, H.; et al. Messinian Salinity Crisis Record under Strong Freshwater Input in Marginal, Intermediate, and Deep Environments: The Case of the North Aegean. *Palaeogeogr. Palaeoclimatol. Palaeoecol.* **2017**, *485*, 316–335. [[CrossRef](#)]
46. Suc, J.-P.; Do Couto, D.; Melinte-Dobrinescu, M.C.; Macaleț, R.; Quillévéré, F.; Clauzon, G.; Csato, I.; Rubino, J.-L.; Popescu, S.-M. The Messinian Salinity Crisis in the Dacic Basin (SW Romania) and Early Zanclean Mediterranean–Eastern Paratethys High Sea-Level Connection. *Palaeogeogr. Palaeoclimatol. Palaeoecol.* **2011**, *310*, 256–272. [[CrossRef](#)]
47. Vigner, A. *Images Sismiques Par Réflexions Verticale et Grand-Angle de La Croûte En Contexte Extensif: Les Cyclades et Le Fossé Nord-Egéen*; Institut de Physique du Globe: Paris, France, 2002.
48. Herron, D.A. *First Steps in Seismic Interpretation*; Society of Exploration Geophysicists: Tulsa, OK, USA, 2011.
49. DUG Insight. *DUG Insight (Version 4.9)*; DUG Technology Ltd.: Perth, Australia, 2021.
50. Sangree, J.; Widmier, J. Seismic Stratigraphy and Global Changes of Sea Level, Part 9: Seismic Interpretation of Clastic Depositional Facies. *Am. Assoc. Pet. Geol. Bull.* **1978**, *62*, 752–771. [[CrossRef](#)]
51. Mitchum, R.M.; Vail, P.R.; Sangree, J.B. Seismic Stratigraphy and Global Changes of Sea Level, Part 6: Stratigraphic Interpretation of Seismic Reflection Patterns in Depositional Sequences. *Seism. Stratigr. Appl. Hydrocarb. Explor.* **1977**, 117–134.
52. Brun, J.-P.; Sokoutis, D. Kinematics of the Southern Rhodope Core Complex (North Greece). *Int. J. Earth Sci.* **2007**, *96*, 1079–1099. [[CrossRef](#)]
53. Brun, J.P.; Sokoutis, D. Core Complex Segmentation in North Aegean, A Dynamic View. *Tectonics* **2018**, *37*, 1797–1830. [[CrossRef](#)]
54. Carras, N.; Georgala, D. Upper Jurassic to Lower Cretaceous Carbonate Facies of African Affinities in a Peri-European Area: Chalkidiki Peninsula, Greece. *Facies* **1998**, *38*, 153–164. [[CrossRef](#)]
55. Mercier, J.L.; Sorel, D.; Vergely, P.; Simeakis, K. Extensional Tectonic Regimes in the Aegean Basins during the Cenozoic. *Basin Res.* **1989**, *2*, 49–71. [[CrossRef](#)]
56. Jackson, M.P.A.; Hudec, M.R. Seismic Interpretation of Salt Structures. In *Salt Tectonics*; Cambridge University Press: Cambridge, UK, 2017; pp. 364–398.
57. Lofi, J.; Déverchère, J.; Gaullier, V.; Gillet, H.; Gorini, C.; Guennoc, P.; Loncke, L.; Maillard, A.; Sage, F.; Thion, I.; et al. Seismic Atlas of the Messinian Salinity Crisis Markers in the Mediterranean and Black Seas. *Mem. Société Géologique Fr.* **2011**, 179, 72.
58. Roveri, M.; Flecker, R.; Krijgsman, W.; Lofi, J.; Lugli, S.; Manzi, V.; Sierro, F.J.; Bertini, A.; Camerlenghi, A.; De Lange, G.; et al. The Messinian Salinity Crisis: Past and Future of a Great Challenge for Marine Sciences. *Mar. Geol.* **2014**, *352*, 25–58. [[CrossRef](#)]
59. Montadert, L.; Letouzey, J.; Mauffret, A. Messinian Event: Seismic Evidence. *Initial Reports Deep Sea Drill. Proj.* **1978**, *42*, 1037–1050.
60. Manzi, V.; Gennari, R.; Lugli, S.; Persico, D.; Reghizzi, M.; Roveri, M.; Schreiber, B.C.; Calvo, R.; Gavrieli, I.; Gvirtzman, Z. The Onset of the Messinian Salinity Crisis in the Deep Eastern Mediterranean Basin. *Terra Nov.* **2018**, *30*, 189–198. [[CrossRef](#)]
61. Anastasakis, G.; Piper, D.J.W.; Kontakiotis, G.; Antonarakou, A.; Foutarakis, P. Evolution of Neogene-Quaternary Sedimentation in the North Ionian Sea Basin during the Last Stages of Continental Collision. *Submitt. Mar. Geol.* **2021**. MARGO-S21-00263.
62. Ferentinos, G. Offshore Geological Hazards in the Hellenic Arc. *Mar. Geotechnol.* **1990**, *9*, 261–277. [[CrossRef](#)]
63. Needham, H.D.; Le Pichon, X.; Melguen, M.; Pautot, G.; Renard, V.; Avedik, F.; Carre, D. North Aegean Sea Trough: 1972 Jean Charcot Cruise. *Bull. Geol. Soc. Greece* **1973**, *10*, 152–153.
64. Armijo, R.; Meyer, B.; King, G.C.P.; Rigo, A.; Papanastassiou, D. Quaternary Evolution of the Corinth Rift and Its Implications for the Late Cenozoic Evolution of the Aegean. *Geophys. J. Int.* **1996**, *126*, 11–53. [[CrossRef](#)]

- 
65. Rohais, S.; Joannin, S.; Colin, J.-P.; Suc, J.-P.; Guillocheau, F.; Eschard, R. Age and Environmental Evolution of the Syn-Rift Fill of the Southern Coast of the Gulf of Corinth (Akrata-Derveni Region, Greece). *Bull. Société Géologique Fr.* **2007**, *178*, 231–243. [[CrossRef](#)]
  66. Lykousis, V. Sea-Level Changes and Sedimentary Evolution during the Quaternary in the Northwest Aegean Continental Margin, Greece. In *Sedimentation, Tectonics and Eustasy: Sea-Level Changes at Active Margins, IAS Special Publication*; Wiley: Hoboken, NJ, USA, 1991; Volume 12, pp. 121–131, ISBN 9781444303896.
  67. Kahle, H.-G.; Straub, C.; Reilinger, R.; McClusky, S.; King, R.; Hurst, K.; Veis, G.; Kastens, K.; Cross, P. The Strain Rate Field in the Eastern Mediterranean Region, Estimated by Repeated GPS Measurements. *Tectonophysics* **1998**, *294*, 237–252. [[CrossRef](#)]
  68. Le Pichon, X.; Chamot-Rooke, N.; Lallemand, S.; Noomen, R.; Veis, G. Geodetic Determination of the Kinematics of Central Greece with Respect to Europe: Implications for Eastern Mediterranean Tectonics. *J. Geophys. Res. Solid Earth* **1995**, *100*, 12675–12690. [[CrossRef](#)]